**Department of Neurobiology**
*Kaeser Laboratory*

**Institute of Biotechnology**
*Department of Life Sciences*

# DISSECTING THE LEVEL OF EXPRESSION AND CLUSTERING OF ACTIVE ZONE PROTEINS AT DOPAMINE AND ACETYLCHOLINE RELEASE TERMINALS

**Final Report for Marshall Plan Scholarship**

*Austrian Marshall Plan Foundation*

*Paulína Nemcová*

*Submitted on: 31.03.2019*

IMC University of Applied Sciences
Institute of Biotechnology
Department of Life Sciences



This research has been supervised by:

Dana Mezricky, Prof(FH) Mag., IMC University of Applied Sciences

Pascal Kaeser, M.D., Harvard Medical School

## Acknowledgements

My gratitude belongs to all members of the Kaeser lab that I had an honour to work with during my stay. I acknowledge their technical assistance, comments and scientific support. Kind approach, patience and support of all lab members guided me every moment of this internship. I am specifically thankful to my external supervisor Pascal Kaeser for designing the project, enabling me this research opportunity, encouragement through every challenging moment and thoughtful suggestions regarding this paper. Thank to Lauren Kershberg for kind explanations and teaching me the core techniques used during this research; preparation of synaptosomes, confocal microscopy and basics of used analytical method. My gratitude belongs also to Changliang Liu for writing the MATLAB code for analysis of confocal images, designing and quantifying tested protein combinations in cholinergic interneurons, as well as his overall help and improvement of the analytical process. Further thank to Aditi Banerjee and Jennifer Wang for maintenance and genotyping of the mouse lines used for this project. I thank to Drs. T. Südhof and S. Schoch for antibodies. Harvard Medical School core facilities supported this project: Neurobiology Imaging, the Neurodiscovery Center.

I would like to express my gratitude also to my internal supervisor and academic advisor Dana Mezricky, who was a great support providing answers for all my questions, critical reading of Bachelor Paper I and II, and was always interested in my scientific progress.

Austrian Marshall Plan Foundation helped to make my stay in the United States feasible. I am thankful that they see the aspiration in undergraduate and graduate students across Austria and support the next generation of scientists.

Finally, my family and friends played an important role. They are the ones that move me forward and give me the strength and continuous encouragement to follow my goals. Thank you!

## Abstract

Implication of dopamine in control of essential brain functions places mesolimbic and nigrostriatal dopamine system among unique neuromodulation systems. Signalling by dopamine is involved in emotion, cognition, reward-related learning and habit formation. The imbalance results in severe pathophysiological and behavioural disorders including Parkinson's disease, Huntington's disease, and drug addictions.

Unlike the synaptic transmission of classical neurotransmitters that is fast with high release probability, release of dopamine was for long time considered to be slow, inaccurate without the presence of specialized release sites called active zones. The body of evidence from biochemical and morphological studies suggested six active zone proteins at the vertebrate synapses. However, diffraction limited microscopy did not allow the dissection of colocalization of these proteins on the nanoscale in dopamine axons. The advances in super resolution microscopy tackled this problem. Liu *et. al* revealed a colocalization between active zone proteins bassoon, ELKS and RIM in 30% of dopamine release sites for the first time. Together with studies indicating high release probability, it is hypothesised that dopamine release requires specialized release machinery coupling $Ca^{2+}$ influx to vesicle fusion.

By employment of advanced imaging techniques on immunolabelled purified synapses, the following paper provides the assessment of level of expression of scaffold Liprin-α proteins in dopamine neurons. In addition, preliminary data for other active zone proteins and synaptic markers will be presented. This paper further focuses on molecular architecture of subtype of neurons regulating dopamine release. Inputs from cholinergic and glutamatergic afferents regulate dopamine release. Neurons releasing glutamate that is categorized as classical neurotransmitter are characterized with the presence of specialized release sites. However, the molecular architecture of cholinergic interneurons has not been described to date. Here, we present the first insights into components of protein assembly that mediate acetylcholine release in cholinergic interneurons.



Keywords: dopamine, acetylcholine, active zone proteins, synaptic transmission, neuromodulation

# Table of contents

# Table of figures

# List of tables

# List of abbreviations

| | |
|---|---|
| 3D SIM | 3D Structured illumination microscopy |
| ACh | Acetylcholine |
| AMPAR | α-amino-3-hydroxy-5-methyl-4-isoxazolepropionic acid receptor |
| AU | Arbitrary units |
| B | Bassoon |
| BLAST | Basic local alignment search tool |
| Cas9 | CRISPR associated Protein 9 |
| CRISR | Clustered Regularly Interspaced Short Palindromic Repeats |
| $Chat^{IRES-Cre}$ | Cholinergic interneuron ribosomal entry site-Cre |
| ChI | Cholinergic interneurons |
| cKO | Conditional KO |
| ChR2 | Channelrhodopsin 2 |
| Cre | Causes recombination |
| DA | Dopamine |
| DAT | Dopamine transporter |
| $DAT^{IRES-Cre}$ | DAT internal ribosomal entry site-Cre |
| DNA | Deoxyribonucleic acid |
| ELKS | Protein rich in amino acids E,L,K,S |
| eYFP | Enhanced yellow fluorescent protein |
| GABA | Gamma-aminobutyric acid |
| Glu | Glutamate |
| HEPES | 4-(2-hydroxyethyl)-1-piperazineethanesulfonic acid |
| HRP | Horseradish peroxidase |
| KD | Knock-down |
| KI | Knock-in |
| KO | Knock-out |
| loxP | Locus of X-over P1 |
| mGluR | Muscarinic glutamate receptors |
| MSN | Medium spiny neurons |

| | |
|---|---|
| nAChR | Nicotinic acetylcholine receptors |
| P | Pellet |
| PAGE | Polyacrylamide gel electrophoresis |
| PBS | Phosphate-buffered saline |
| POI | Protein of interest |
| PSD95 | Postsynaptic density 95 |
| RIM | Rab3-interacting molecule |
| RIM-BP | RIM-binding partner |
| RNA | Ribonucleic acid |
| ROI | Region of interest |
| RT | Room temperature |
| S | Supernatant |
| SAM | Sterile alpha motif |
| ScRNA-seq | Small conditional RNA sequence |
| SDS | Sodium-dodecyl sulphate |
| SN | Substantia nigra |
| SNR | Signal to noise ratio |
| STED | Stimulated emission depletion |
| STORM | Stochastic optical resolution |
| STR | Striatum |
| SYP | Synaptophysin |
| tdTomato | Tandem dimer tomato |
| TH | Tyrosine hydroxylase |
| vAChT | Vesicular acetylcholine transporter |
| vGAT | Vesicular GABA transporter |
| vGluT1 | Vesicular glutamate transporter 1 |
| VTA | Ventral tegmental area |
| WT | Wildtype |

# List of URLs

| | |
|---|---|
| Allen Brain Atlas | http://portal.brain-map.org/ |
| DropViz | http://dropviz.org/ |
| ImageJ | https://imagej.nih.gov/ij/ |
| MATLAB | https://www.mathworks.com/products/matlab.html |
| MATLAB code | https://github.com/hmslcl/3D_SIM_analysis_HMS_Kaeser-lab_CL |
| Prism | https://www.graphpad.com/scientific-software/prism/ |

# 1 Introduction

## 1.1 Dopaminergic and cholinergic neuron system

Dopamine (DA) system is involved in goal directed behaviour, emotion, cognition, dysfunction of which is leading to multitude of disorders including schizophrenia and depression (Brichta et al., 2015; Grace, 2016; Surmeier, Graves, & Shen, 2014). Difference between motivational behaviour and salience is encoded in modes of DA neuron firing. The parallel research of multiple groups resulted into hypothesis stating the dependence of behavioural selection on the switch between slow tonic and intermittent burst firing (Grace, 2016). Despite action potential in DA neurons is the principal activator of DA release, the striatal cholinergic interneurons (ChI) play a significant role in this process as well. DA release is controlled through firing of neurons located in substantia nigra (SN) and ventral tegmental area (VTA), however, the release is also locally influenced by direct actions in the striatum (Cachope & Cheer, 2014). Endogenous glutamatergic and cholinergic activity can trigger DA release independent of cell body firing. Striatal ChI that account for 2-5% of striatal neurons provide the acetylcholine (ACh) that is binding to β-subunits of nicotinic receptors localized on DA axons (Figure 1). Pauses in DA release also correlate with pauses in ACh release and the effect next DA neuron depolarization with reduced release probability but increased gain of signal (Threlfell et al., 2012).

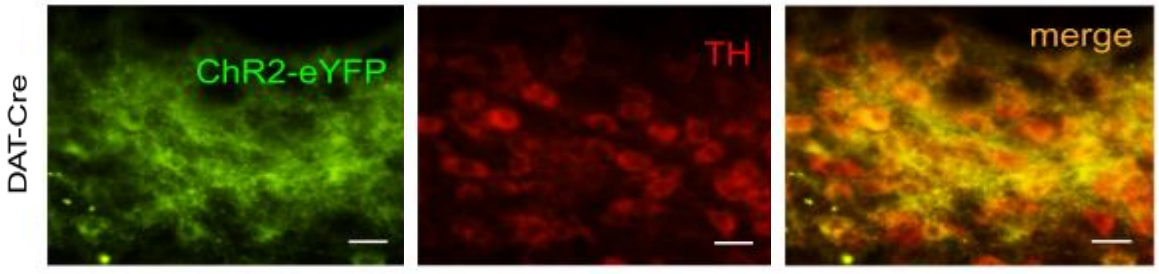


**Figure 1: Coexpression of cholinergic and dopamine neurons.**

Light-activated ion channel channelrhodopsin2 (ChR2) incorporated into mouse striatal ChI with expression limited to subset of ChI fused with light activated enhanced yellow fluorescent protein (eYFP) under the control of promoter for enzyme producing ACh, choline acetyltransferase. DA neurons were identified with the presence of DA synthetising enzyme, tyrosine hydroxylase (TH). Scale bar: 20 um. Source referring to: (Threlfell et al., 2012).

## 1.2 Termino-terminal control of dopamine release

Excitatory stimulation of DA axons in the striatum is originating from the cortex, amygdala and hippocampus. Inhibitory gamma-aminobutyric acid (GABA)-ergic transmission is arising from VTA and ventral pallidum (Tritsch, Ding, & Sabatini, 2012). In contrast, cell bodies of ChI residing in brainstem send their axonal projections to the striatum. Similarly, as dopaminergic neurons, characterized with relatively low rate of firing, inputs from terminals of these neurons encode reward-related processes. Released ACh is binding to muscarinic and nicotinic receptors. Striatal DA axons express high density of subunits of nicotinic receptors. Cholinergic control of DA release is mediated through high binding affinity of ACh to β2 subunit on striatal DA axons with the subsequent initiation of DA release (Cachope & Cheer, 2014; Cachope et al., 2012; Jones, Bolam, & Wonnacott, 2001), (Figure 2).

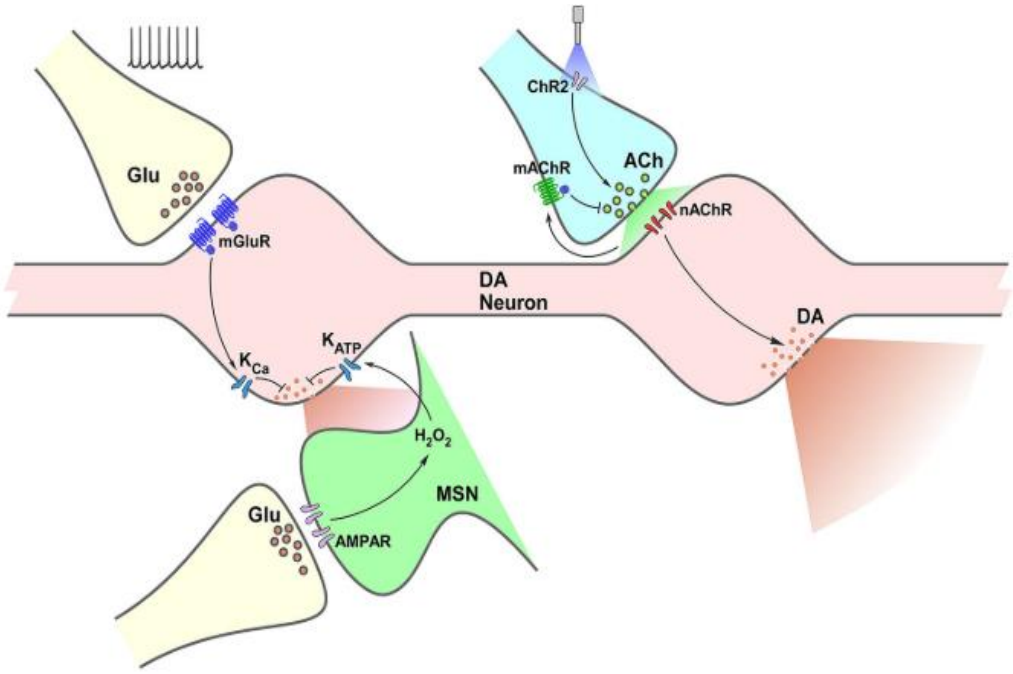


**Figure 2: Inputs from terminals of different neuronal subtypes.**

Glutamatergic (Glu; yellow) and cholinergic (ACh; blue) terminals can execute DA release without dopaminergic cell body firing. Similarly, actvation of receptors on medium spiny neruons (MSN; green) is resulting in elevated production of hydrogen peroxide that is further diffusing to DA varicosities resulting in inhibition of DA release. Optogenetically activated cholinergic interneuons through ChR2 release acetylcholine (ACh) that subsequently triggers DA release upon its binding on nicotinic recepotors (nAChR). Source referring to: (Cachope & Cheer, 2014).

## *1.3 In situ* hybridization of transcriptome of adult mouse brain

Integration of neuroanatomical, genetic and connectivity experiments provide supporting data for further hypotheses driven research. Allen Brain Atlas has merged and displayed the datasets of *in situ* hybridization of 20 000 genes, histology, microarray, RNA sequencing, projection mapping and magnetic resonance imaging in coronal and sagittal brain sections (Figure 3). This is providing the transcriptomic profile with cellular resolution. Data are organized as neuroBlast search that is a reference to the Basic Local Alignment Search Tool (BLAST), (Sunkin et al., 2013).

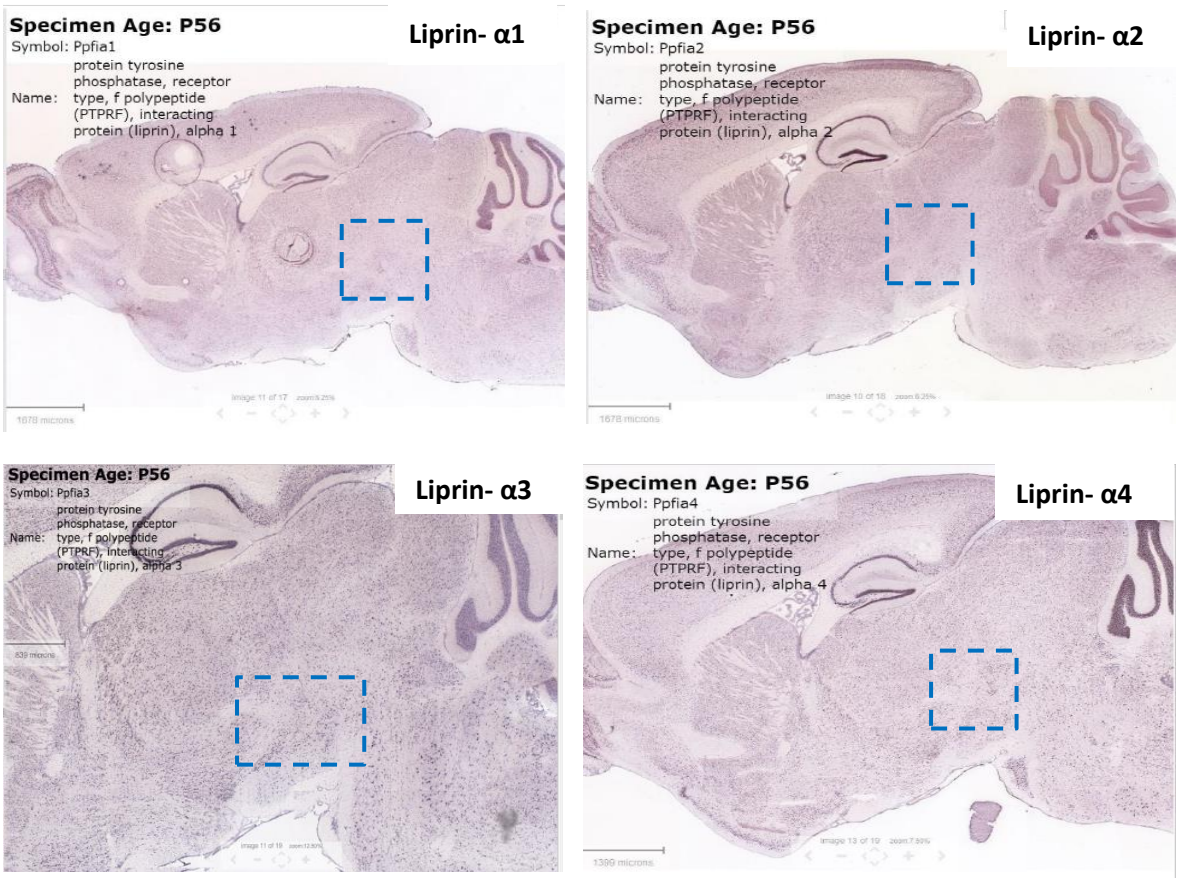


**Figure 3: Neuroanatomical gene expression in dopamine related basal ganglia.**

Liprin-α3, a protein isoform with expression restricted only to brain tissue shown in saggital section of mouse brain after postnatal day 56 (P56). The expression level of Liprin-α2 is depicted less reduntant, however, this isoform is similarly characterized with expression only in brain tissue. In comparison, profiles of other two isoforms of this protein do not show region with darker, solid structures indicating increased level of expression. The approximate estimation of the investigated brain region illustrated in blue. Source modified after: “Allen Brain Atlas”, http://www.brain-map.org.

## 1.4 Single cell transcriptome of adult mouse brain

DropViz is a single-cell database of cell types, states and transcriptional patterns (Figure 4). High-throughput technology of genome transcript counting named Drop-seq is applied to single-cell suspensions for the sequencing of 690 000 cells from nine brain regions of adult mouse. Small conditional ribonucleic acid (ScRNA)-seq studies have identified also a group of principal neurons in the striatum that was not identified before despite the extensive research. Immediate early genes are responsible for neuronal cellular response and are characterized with uniform expression profile across different neuronal subtypes. This group of genes is the appropriate target for Drop-seq detection. Outcomes of these studies summarize the conserved transcriptional program within various neuronal types for genes involving maintenance, expansion or subcellular axonal transport, as well as transport to presynaptic terminal. In contrast, neurons with extensive axonal branching or fast rates of firing are characterized with specific transcriptional program (Saunders et al., 2018).

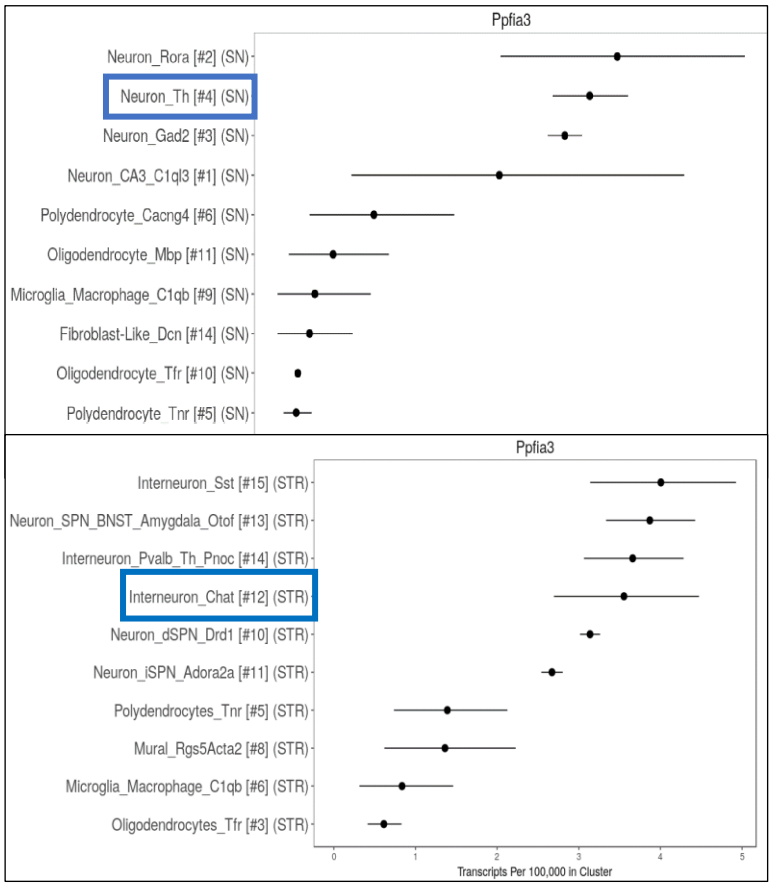


**Figure 4: Clusters with the highest expression of gene Ppfia3 encoding active zone protein Liprin-α3.**

The expression profile of Ppfia3 is compared across various neuron clusters in substantia nigra (SN). Specific focus is pointed towards DA neuron cluster designated as Neuron_Th respresenting the level of RNA expression in this subset of neurons. RNA level of Liprin-α3 was assesed in the striatum (STR) where the interest is in the cholinergic interneurons cluster labelled Interneuron_Chat. These datasets of RNA sequence provide supportive references for the assesment of protein level described in this paper. Source modified after: “DropViz”, http://dropviz.org/

## 1.5 Core active zone proteins

Molecular ultrastructre of presynaptic terminal accelerating vesicle fusion for fast synaptic transmission is composed of evolutionarily conserved protein complex. Neurotransmitters are released upon action potential triggered opening of voltage-gated $Ca^{2+}$ channels. Body of literature resulting from biochemical and morphological studies has identified core active zone proteins ELKS - proteins rich in amino acids E,L,K,S; Liprin-α proteins, Rab3 interacting molecules (RIMs), RIM-binding partners (RIM-BPs) and Munc13s within the cytomatrix of presynaptic terminal. Unlike other enriched active zone proteins, homologous scaffolds bassoon and piccolo are not evolutionarily conserved, thus can be identified only at vertebrate synapses (Dani, Huang, Bergan, Dulac, & Zhuang, 2010; Sudhof, 2012).

## 1.6 Protein composition of dopamine release sites

### 1.6.1 Molecular scaffold bassoon

Fast synaptic neurotransmission is characterized with the presence of specialized release site in a form of active zone with bassoon as the scaffold of this protein assembly (Altrock et al., 2003). Release of DA was for long time considered to be inaccurate, widespread, not requiring the presence of specialized release hotspots. Based on these properties, the extrasynaptic localization of DA receptors and G-protein coupled receptor signalling that is operating comparably slower than ionotropic receptor signalling, DA was categorized as volume transmitter (Table 1), (Agnati, Zoli, Stromberg, & Fuxe, 1995). However, recently Liu *et. al* has demonstrated the presence of the molecular scaffold protein bassoon in DA axons by employment of 3D structured illumination (3D-SIM) microscopy enhancing the resolution in all three dimensions. Furthermore, immunostaining with the antibodies against vesicular marker synaptobrevin-2, bassoon and tyrosine hydroxylase (TH) revealed colocalization pattern indicating that DA neurons contain vesicle clusters that are associated with active zone proteins (Liu, Kershberg, Wang, Schneeberger, & Kaeser, 2018).

**Table 1: Modes of interneuron communication.**

Basic properties of two modes of interneuron communication are shown. Source modified after: (Agnati et al., 1995; Hirase, Iwai, Takata, Shinohara, & Mishima, 2014)

| | Wiring transmission | Volume transmission |
|---|---|---|
| **Concentration of signal** | usually high | usually low |
| **Affinity of receiver** | usually high | usually low |
| **Release site to target link** | 1:1 link | 1:n link (n>>1) |
| **Speed of transmission** | high | low |
| **Safety of transmission** | high | usually low |
| **Energy cost** | high | usually low |

### 1.6.2 Redundant active zone proteins RIM and ELKS

Other two redundant active zone proteins RIM and ELKS were tested in previous studies using conditional knockout (cKO) mice with removed isoforms of these proteins specifically from DA neurons. Colocalization with dopamine transporter (DAT) responsible for DA pumping out of synaptic cleft, was demonstrated to be high in TH-positive cells independent of the presence of bassoon. Due to chromatic aberration of 3D-SIM microscopy that limits the imaging only up to two colours, confocal microscopy is an alternative approach. The artifact of immunostaining is determined by evaluation of detected clusters in cKO mice. Dataset obtained from these experiments together with the body of evidence indicating the extensive binding partners of RIM and ELKS proteins establish the presence of RIM, ELKS and bassoon in DA neurons. Furthermore, amperometry in brain slices tested the functional aspect of active zone mediated release. Biphasic DA release was triggered 20% by action potential, whereas 80% was triggered by coactivated cholinergic afferents (Liu et al., 2018). In contrast, amperometry in slices prepared from RIM cKO$^{DA}$ mice resulted in no detectable DA release. Applying the same methodology for testing of roles of ELKS in DA release, strikingly, resulted in no effect on level of detected DA release. Besides amperometry, the role of RIM in DA neuron morphology, synthesis

and vesicular loading was tested. No obvious defects in neuron development or change to tissue DA levels were detected. This excludes the possibility of misinterpreted explanation of RIM cKO$^{DA}$ mice with abolished DA release. Finally, it was hypothesized that proteins for synaptic vesicle fusion Munc13 and Munc18 might be affected by removal of RIM. This hypothesis was not confirmed. Thence, the loss of DA release is not a consequence of mismatched assembly of multiple proteins. Fast release probability detected in electrophysiological recordings supports the requisite of scaffolds connecting the influx of $Ca^{2+}$ to $Ca^{2+}$ sensors and release-ready vesicles. Outcomes of these experiments show that RIM is the organizer of protein assembly at DA release sites (Liu et al., 2018).

### 1.6.3 Sparse distribution of release sites in dopamine axons

Comparing the frequency distribution of release sites in axons of fast neurotransmitters, release sites in DA axons are sparsely present with distribution of clusters being encountered in frequency of 1 cluster per 4 µm of axonal length (Figure 5). Analysis of this distribution revealed that only 30% of vesicle clusters are associated with the presence of active zone release sites. The distribution in TH-negative cells, representing axonal projections of any neuronal cell type besides dopaminergic, reaches the level of approximately 50% of vesicle cluster associated with active zones. In summary, DA nerve terminals are characterized with specialized active zone release sites to a comparably less frequent extent than glutamatergic nerve terminals (Liu et al., 2018).

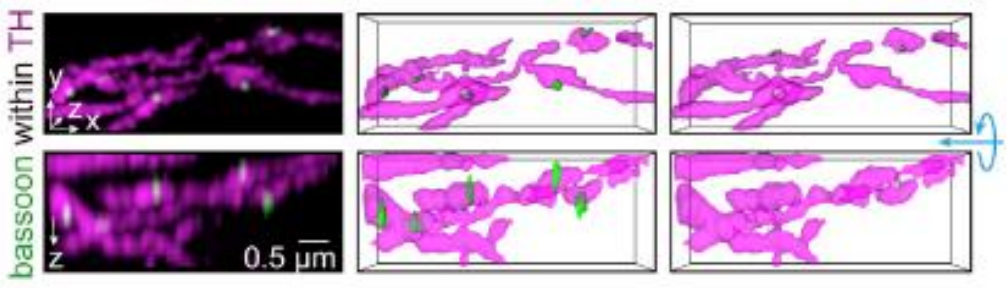


**Figure 5: Sparse distribution of bassoon on dopamine axons.**

3D superresolution images of brain slices from dorsal striatum show a distribution of bassoon clusters. Images are followed 90° rotation around x-axis. Source referring to: (Liu et al., 2018).

## 1.7 Synaptosomes

Synaptosomes - a term created by Victor Whittaker - are isolated fractions of synaptic terminals that are membrane enclosed (Whittaker et al., 1964), (Figure 6). This approach simplifies the complex network of mammalian brain that is composed of neural, non-neural tissue, as well as blood vessels. It is a method widely used for the study of synaptic processes. However, the drawback of experiments undertaken in material processed this way is the simultaneous content of extrasynaptic and non-synaptic tissue such as glial cells and debris particles. The heterogeneity relates to multiple types of synaptic connections, and up to 50% of non-neuronal particles. This isolated synaptic terminal is composed of synaptic vesicles, mitochondrion and post-synaptic density, and comprises all functional properties (Biesemann et al., 2014).


**Figure 6: Isolated membrane enclosed synaptic boutons – synaptosomes.**

Upon disruption of nerve cells in the solution isotonic to plasma membrane, the synaptic boutons resist disruptive forces and start forming individual membrane enclosed structures. One or multiple mitochondria might be included in these structural units as the number of mitochondria is generally higher near the vicinity of synaptic boutons due to increased energy demands for synaptic transmission. Postsynaptic density might be also encountered if the higher protein density of this synaptic part sustains the disruptive forces. Further subcellular components comprise synaptic vesicles that can be purified in separated process. The heterogenity is the result of presence of non-neural tissue, multiple types of neurons and debris particles. Source referring to: (Biesemann et al., 2014).

Application of this method is possible since homogenization in detergent-free media isosmotic to plasma membrane allows presynaptic nerve terminals to resist disruptive forces. Instead of disruption, the formation of preserved distinct compartments is initiated. The presence of neurotransmitters such as ACh, hydroxytryptamine, noradrenaline or DA indicates the presence of synthetizing enzymes located in the specific type of neurons. The characteristic appearance as observed under electron microscope after staining and thin sectioning is a thin-walled round shape with

cytoplasm, synaptic vesicles and granules, sometime with one or more mitochondria. Post-synaptic density is a thicker region, however, in some cases may still resist the homogenization and accompany the synaptosome. Preparation of synaptosomes in hypoosmotic buffer causes in majority the burst of synaptosomes. However, synaptic vesicles remain intact even upon the homogenization in hypoosmotic buffer. In contrast, freezing and thawing eliminates synaptosome rupturing but almost abolishes the presence of intact synaptic vesicles. This allows specific fractionation of synaptosomes based on structures of interest into subfractions of synaptic vesicles, soluble cytoplasm, mitochondria and post-synaptic density (Whittaker, Michaelson, & Kirkland, 1964).

### 1.7.1 Microsomes

The structure formed as contamination to original synaptosome fraction. It is an artifact of an enclosure of larger structure during the process of disruption. The markers for soluble cytoplasm and mitochondria have been used as determinant of this substructure (Whittaker et al., 1964).

## 1.8 Mouse genetics

### 1.8.1 Cre recombination

Manipulating protein expression specifically in subset of cells is a valuable scientific methodology eliminating the consequence of frequent embryonic lethal stage resulting from complete removal present in constitutive knockout animal models (KO). Site-specific recombinase Cre - as abbreviated for Causes recombination - originating from P1 bacteriophage catalyses the recombination between two recognition locus of X-over P1 (loxP) sites (Backman et al., 2006). Recognition sites are flanked by two palindromic sequences and asymmetric core spacer sequence. The asymmetry determines the orientation of the recombination site. The recombination mechanism is undertaken within the spacer area in a way of single recombinase molecule binding to loxP sites followed by tetramer formation (Nagy, 2000). The Cre-loxP recombination system is referred to as CAG promoter-driven loxP-STOP-

loxP system. Experimental set-up described in this paper was performed using mouse animal models with removed specific active zone proteins or with expression of marker proteins specifically in DA neurons by dopamine transporter internal ribosomal entry site-Cre ($DAT^{IRES\text{-}Cre}$) or cholinergic interneurons by choline acetyltransferase internal ribosomal entry site-Cre ($Chat^{IRES\text{-}Cre}$). For this purpose, the used experimental models are bicistronic Cre recombinase knock-in (KI) mice with expression from DAT or Chat gene locus. Conditional KO of RIM proteins is resulting from crossing previously generated RIM1 and RIM2 double floxed mice with $DAT^{IRES\text{-}Cre}$ mice (Liu et al., 2018). In contrast, constitutive KO of Liprin-α3, also referred to as conventional or whole-body KO, is not restricted to a subset of nerve cells. This mouse line was generated by clustered regularly interspaced short palindromic repeats/CRISPR-associated protein 9 (CRISPR/Cas9) mediated gene editing in single cell zygotes. Wong *et al.* induced frame-shift mutation through allele with 8-bp deletion consequently resulting in nonsense-mediated decay. Mice with constitutive KO of Liprin-α3 are viable and fertile, the only observed abnormalities are in open space locomotion (Wong et al., 2018).

### 1.8.2 Transgenic animal models

The rationale of Cre recombination can be applied not only for the cell-type restricted protein removal but for further extended purposes. For multitude of experimental approaches synaptic vesicles identified with vesicular markers such as membrane-spanning protein synaptophysin (SYP) can be specifically labelled in a subset of cells. Mice with SYP-tandem dimerTomato (tdTomato) cassette and Cre-loxP recombination system (SYP-tdTomato) in Rosa26 gene locus are crossed with mice expressing markers of neuronal subtypes. For the labelling of ChI, SYP-tdTomato mice were crossed with neuronal subtype marker expressing $Chat^{IRES\text{-}Cre}$ mice (Liu et al., 2018). Rosa26 locus is widely used locus because of its high level of expression in most cells and tissues of adult mice with an exception of some postmitotic neurons that have lower level of expression. It is located on the chromosome 6 and was identifies by random gene-trap screening in retrovirus ROSABgal (Kobayashi et al., 2012).

## 1.9 Confocal laser scanning microscopy

Imaging microscopic techniques and their advancements are a crucial aspect of biological research revealing structure on micro- to nanoscale. Samples used for confocal imaging are either living or fixed tissues with fluorescently labelled probes. Under conventional light microscope, the fluorescent light interferes with the resolution. Confocal microscope provides increased resolution in both, axial and lateral direction by means of out-of-focus light elimination. Confocal microscope is providing the maximum resolution of 0.2 um detecting emissions from 400 to 700 nm, whereas the resolution of transmission electron microscope is 0.1 nm. The device is composed of laser light source, photomultiplier tube detector and controller of scanning mirrors. Image acquisition is performed in a way of optical sectioning. During this process the sample is scanned with one or more focused laser beams. The higher the magnification of the objective lens and the narrower the pinhole diameter, the higher the resolution (Paddock, 1999, 2000; Paddock & Eliceiri, 2014).

## 1.10 Superresolution microscopy techniques

Imaging of the protein structure and its subcellular distribution on the nanoscale is possible with advanced photon microscopy techniques such as stimulated emission depletion (STED) or stochastic optical resolution (STORM). These techniques are based on depletion of the selected fluorophores, thus targeted switching, or selected photoactivation as in the case of STORM. Excitation and depletion lasers are forming a doughnut shape in their overlapped excitation in the focal plane of STED microscope forming a high-resolution probe scan. The resolution is 3-fold higher than in confocal microscopy (Paes, Habrant, & Terryn, 2018).

## 1.11 Monoclonal and polyclonal antibodies

### 1.11.1 Basic properties

Introducing antigens into animals results in the formation of host proteins - antibodies composed of heavy and light chains. Hapten – a substance not inducing antibody

formation – is used for the determination of the portion of antibody combination site. Antigenic determinants such are repeating units of linear polysaccharides, multiple terminal in branched polysaccharide, projecting sequence of amino acids, nucleotides in polynucleotides, RNA and deoxyribonucleic acid (DNA), and others. These properties categorize used antibodies into antibody populations with differing specificities. Ultimately, the accessibility to antibody combining site determines the reactivity properties (Kabat, 1980; Zhong, Reis e Sousa, & Germain, 1997). Monoclonal antibodies produced as clones of original parent B lymphocytes are characterized with the binding capabilities to the same epitope. In comparison, polyclonal antibodies are produced in several different lines of B lymphocytes and are recognizing multiple epitopes on the antigen (Tabll, Abbas, El-Kafrawy, & Wahid, 2015).

### 1.11.2 Novel approaches

Recombinant antibodies and single domain antibodies called nanobodies are new developed ways of increasing specificity of antibody binding capabilities, level of tissue penetration, circumventing problems with cell-line drift and mutations as well as overall ease of production (Pardon et al., 2014; Schenck et al., 2017).

## 1.12 Research question and aim of the project

Unlike the synaptic transmission of classical neurotransmitters that is fast with high release probability, the mode of DA signalling was long considered to be slow and inaccurate, and hence it was thought that it does not require specialized machinery for fast release. Recently, Liu *et al.* identified that DA release is restricted to active zone-like release sites, which consist of machinery that accelerates DA secretion and restricts it to a few hot spots. However, only three components of this release site are known: RIM, bassoon and ELKS2. It is hypothesized that other known active zone proteins control dopamine release. The main goal underlies the assessment of the level of expression of Liprin-α and other active zone proteins at the DA release sites. Simultaneously, investigated brain region - striatum - encounters innervation by local ChI releasing ACh together creating an interwound network. In addition to the main goal, the interest is to determine whether ACh release sites are also

characterized with the presence of active zone proteins. The research questions delineate whether Liprin-α proteins are expressed and clustered at DA release sites, what other active zone proteins are involved in spatiotamporal control of DA release and whether active zone proteins are present at ACh release sites.

# 2 Material and Methods

## 2.1 Striatal synaptosome preparation

Adult mice (postnatal day 21-70) were deeply anesthetized with isoflurane. The animals were decapitated, brain was exposed, cooled down with ice-cold Dulbecco's Phosphate-Buffered Saline (PBS), cut in half along the midline, hipoccampus and cerrebelum were discarded and striatum was scraped out from the cortex. Dissected striatum was placed into pre-cooled glass Teflon homogenizer and 1 ml of ice-cold homogenizing buffer containing (in mM) 4 4-(2-hydroxyethyl)-1-piperazineethanesulfonic acid (HEPES), 320 sucrose, and 1x protease inhibitor cocktail, pH 7.4 was added to the homogenizer.The tissue was homogenized with 12 strokes. After homogenization, additional 1 ml of homogenizing buffer was added. The homogenate was centrifuged at 1,000 g (Fiberlite™ F15-6 x 100y Fixed-Angle Rotor) for 10 min at 4°C. The supernatant (S1) was aspirated and centrifuged at 12,500 g for 15 min at 4°C. The supernatant (S2) was removed and the pellet (P2) was rehomogenized in 1 ml of homogenizing buffer with 6 strokes. After homgenization, additional 1 ml of homogenizing buffer was added. The homogenate of P2 was loaded in volume of 1.5 ml on the top of Ficoll sucrose density gradient made of 5 ml 1.2 M sucrose and 5 ml 0.8 M sucrose in tubes for ultracentrifugation (tube, thinwall, ultraclear 13.2 mL, 14x89 mm, Beckman coulter, cat. nr. 344059). The sample was centrifuged at 69,150 g (SW 41 Ti Swinging-Bucket Rotor, Beckman coulter, cat. nr. 331362) for 70 min at 4°C. The synaptosome layer was harvested in volume of 1-1.5 ml from the interface of two sucrose layers.

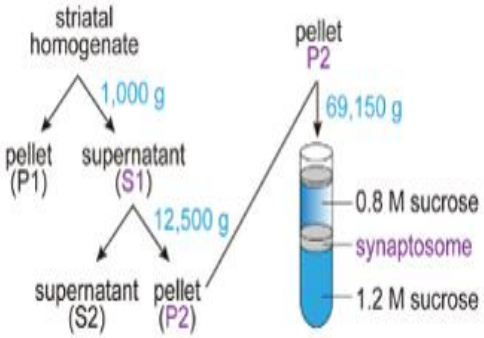


**Figure 7: Purification of striatal synaptosomes.**

The fractions are purified from Ficoll density gradient based on differential centrifugation steps. Electron microscopy revealed that ~60% of the fractionated organelles are synaptosomes loaded with synaptic vesicles, mitochondria comprise ~20% and myelin ~8%. Source referring to: (Biesemann et al., 2014; Liu et al., 2018; Wilhelm et al., 2014).

## 2.2 Processing of striatal synaptosomes

### 2.2.1 Western Blotting

Striatal homogenate, as well as fractions from intermediate steps (S1, S2, P1, P2) were diluted 6-fold with homogenizing buffer. This step equalized the concentration of myelin, 0.8 M sucrose, synaptosome, 1.2 M sucrose and pellet fractions harvested from Ficoll density gradient. The fraction of pellet harvested after ultracentrifugation was snap frozen in dry ice and rehomogenized. The samples were subsequently boiled in 3X sodiumdodecyl sulphate (SDS) buffer for 10 min. Samples were run on sodium dodecylsulphate polyacrylamide (SDS-PAGE) gel with prestained ladder followed by transfer on nitrocellulose membrane. Membranes were blocked in filtered 10% nonfat milk containing 5% goat serum for 1 h at room temperature. Diffent combination of primary and secondary antibodies (Table 2) was incubated in 5% nonfat milk containing 2.5% goat serum for 2  and 1 h at room temperature, respectively. Western blots were imaged in different exposure times after chemiluminescent enhancement witth horseraddish peroxidase (HRP) coupled to secondary antibodies.

**Table 2: Antibodies used in this study.**

Target proteins of antibodies, the andibody source, RRID and dilutions are shown. Source: author's chart.

| REAGENT | CONCENTRATION | SOURCE | IDENTIFIER |
|---|---|---|---|
| **Primary antibodies** | | | |
| Mouse anti-β-actin | 1:2,000 | Sigma | Cat#: A1978-200UL<br>RRID: AB_476692 |
| Rabbit anti-panELKS | 1:1,000 | Liu et al., 2014 (gift from Dr. Sudhof) | Cat#: P224<br>RRID: n.a. |
| Rabbit anti-synaptobrevin-2 | 1:1,000 | Synaptic Systems | Cat #.: 104 202<br>RRID: AB_887810 |
| **Secondary antibodies** | | | |
| HRP- mouse | 1:10,000 | Cappel | 55550 / 04346 |
| HRP- rabbit | 1:10,000 | Cappel | 55550 / 04346 |

### 2.2.2 Fluorescent immunocytochemistry for confocal microscopy

Striatal synaptosomes were diluted 20-30 times in homogenzing buffer to obtain suspension with low density for plating. Diluted synaptosomes were pippeted in the volume of 1 ml into 12-well plate with inserted #1.5 coverglasses coated with poly-d-lysine. The sample was spun down on coverglasses at 4,000 g for 10 min at 4°C. Excess homogenizing buffer was aspirated and synaptosomes were fixed on the coverslips in solution of 4% paraformaldehyde in phosphate buffered saline (PBS) for the duration of 10 min. Fixing reaction was stop with two 10 minutes washes in PBS. Purified synaptosome fraction was kept on ice and in detergent-free environment up to post-fixative processes. Blocking and permeabiliztaion for 45 min at room temperature (RT) were performed with the addition of 3% bovine serum albumin in PBS and 0.1% Triton X-100 in PBS, respectively. Samples were further immunostained with selected set of primary and fluorescent secondary antibodies (Table 3). Primary antibodies were used for 12 h at 4°C, fluorescent secondary antobodies were used for 2 h at RT in blocking solution. Series of 5 min washing steps were applied after each staining to remove unbound antibodies. Prior mounting, coverslips were rinsed with distilled water to avoid PBS precipitation. Coverslips were mounted on the slides with Fluoromount-G (SouthernBiotech). Samples were left in dark for 12 h to dry. Photobleaching of secondary antibodies was avoided by usage of aluminium foil and storage in light-tight container.

**Table 3: Fluorescent antibodies used in this study.**

Target proteins of antibodies, the andibody source, RRID and dilutions are shown. Source: author's chart.

| REAGENT | CONCENTRATION | SOURCE | IDENTIFIER |
|---|---|---|---|
| **Primary antibodies** | | | |
| Guinea pig anti-TH | 1:1000 | Synaptic Systems | Cat# 213104; RRID: AB_2619897 |
| Guinea pig anti-vGAT | 1:1000 | Synaptic Systems | Cat# 131 004 RRID: AB_887873 |
| Guinea pig anti-vGluT1 | 1:1000 | Synaptic Systems | Cat# 135 304 RRID: AB_887878 |
| Mouse anti-bassoon | 1:1000 | Enzo life sciences | Cat# ADI-VAM-PS003-F; RRID: AB_11181058 |

| | | | |
|---|---|---|---|
| Mouse anti- ELKS1α A/B | 1:500 | Santa Cruz | Cat# sc-365715 RRID: AB_10841908 |
| Mouse anti-ELKS1/2α | 1:1000 | Abcam | Cat# ab50312 RRID: AB_869944 |
| Mouse anti-PSD95 | 1:1000 | Neuromab | Cat# 73-028 RRID: AB_10698024 |
| Mouse anti-synapotphysin | 1:1000 | Synaptic Systems | Cat# 101 011 RRID: AB_887824 |
| Rabbit anti-DAT | 1:1000 | Millipore | Cat# AB1591p RRID: AB_90808 |
| Rabbit anti-ELKS2α | 1:100 | Held et. al, 2016 | Cat# 1029 RRID: AB_887733 |
| Rabbit anti-Munc13-1 | 1:1000 | Synaptic Systems | Cat# 126103 RRID: AB_887733 |
| Rabbit anti-Liprin-α2 | 1:50 | Wang et. al, 2016 (gift from Dr. Schoch) | Cat# n.a. RRID: n.a. |
| Rabbit anti-Liprin-α3 | 1:1000 | Wong et. al, 2018 (gift from Dr. Sudhof) | Cat# 4396 RRID: AB_2617056 |
| Rabbit anti-piccolo | 1:1000 | Synaptic Systems | Cat# 142 002 RRID: AB_887759 |
| Rabbit anti-RIM | 1:1000 | Synaptic Systems | Cat# 140 003 RRID: AB_887774 |
| Rabbit anti-RIM-BP2 | 1:1000 | Wang et. al, 2016 (gift from Dr. Sudhof) | Cat# 4193 RRID: n.a. |
| Rabbit anti-synaptotagmin1 | 1:1000 | Pang et. al, 2006 (gift from Dr. Sudhof) | Cat# V216 RRID: n.a. |
| Rabbit anti-vAChT | 1:1000 | Synaptic Systems | Cat# 139103 RRID: AB_887864 |
| **Secondary antibodies** | | | |
| Anti-mouse Alexa Fluor-488 | 1:500 | Thermo Fisher | Cat# A-21131 RRID AB_2535771 |
| Anti-mouse Alexa Fluor-488 | 1:500 | Thermo Fisher | Cat# A-21121 RRID: AB_2535764 |
| Anti-rabbit Alexa Flour-555 | 1:500 | Thermo Fisher | Cat# A-21428 RRID: AB_2535849 |
| Anti-guinea pig Alexa Fluor-633 | 1:500 | Thermo Fisher | Cat# A-21105 RRID: AB_2535757 |

## 2.3 Image acquisition and processing

Images of striatal synaptosomes labelled with fluorescent antibodies were acquired with the confocal laser scanning microscope (FV1000, Olympus). Paramenters for the image acquisition were set specifically for each sample. Imaging of synaptosomes prepared from KO mice and littermate WT mice were imaged under the same acquisition settings with the experimenter blinded to genotype. Laser transmissivity and voltage were set to avoid signal saturation with optimized selection of lower transmissivity and higher voltage. Kalman line filtering mode was applied in order to average out the noise signal and improve the signal to noise ratio (SNR). Scanning speed of 8-10 us/pixel and average count for Kalman filter of 2 or 3 were applied, since exceeding these parametric values might result in sample bleaching. Lasers were chosen corresponding to the excitation wavelength of used secondary antibodies. Photomultiplier detection units were controlled through adjustments of laser gain and offset. Increasing the gain amplifies the strongest signal without amplifying the weakest. However, this approach would result in biased signal detection, thus was not used in any case. Increasing the offset minimizes background noise, however, improper use of this function results in masking of the real signal. The level of offset was established each time under high-low view. Resolution was used at 1024 x 1024 pixels with objective carrying magnification of 60x. When necessary to improve SNR, Leica TCS SP8 STED microscope was used in confocal mode increasing resolution to 2048 x 2048 pixels with objective carrying magnification of 63x. Images were sequentially scanned, detection of signal from each secondary antibody was outputted into separated channels. Acquired images were processed in NIH ImageJ software with the adjustment of colour, brightness and contrast.

## 2.4 Image segmentation

Obtained images were analzyed by multistep experimental approach (Figure 8). Since imaging of synaptosomes is effective only within one focal plane of width ~500 nm, acquired images might contain area out of focus. This would directly effect the analysis, thereby each image was inspected and the region of interest (ROI) was

cropped out. Cropped focused areas were background substracted with rolling ball radius algorithm fitting the size of synaptosomes, as this factor is dependent on the resolution and selected optical zoom. This algorithm is averaging an area of the rolling ball with subsequent subtraction of this value. This is a follow-up step after Kalman filtering that is removing background staining and uneven illumination. Background subtracted images were further viewed with under different thresholding values that were manually selected in order to segment the real signal from noise.

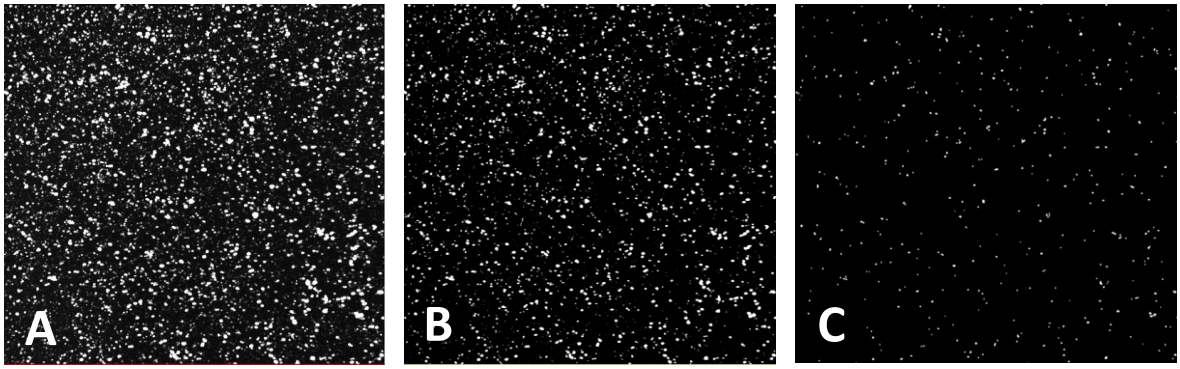


**Figure 8: Stepwise image processing overview.**

Out of focus areas were cropped out (A), image was further processed with background subtraction algorithm subtracting the average value of area of rolling ball (B). Applying selection criteria such as aspect ratio, pixel number and intensity cut-off based on threshold value segment the real signal from noise (C). Outputted images are compared with original or background subtracted images as a control avoiding the selection of false positives. Frequency distribution of signal in outputted masked images is tested in histograms and profile plots as an additional experimental quality control. Source: author's chart.

## 2.5 Object detection by thresholding

Applying global thresholding algorithms such as Otsu that are creating binary images did not result in succesful object recognition in case of synaptosomes. Otsu thresholding method is optimized for segmentation of images with greater object versus background difference, as well as size of the object as in case for neuronal cultures or brain sections. As the wrong choice of threshold would result in different interpretation due to false positives, this step was repeated more times and generated masked images were compared with original background substracted images.

### 2.5.1 Regions of interest

Five different groups of ROIs were generated (Figure 9). ROIs that contain overlap of the protein of interest (POI) in the active zone marker bassoon (B), and marker of subsets of DA neurons - enzyme TH, this is the representation of the level of POI at active zones in DA neurons. Restricting ROIs only to POI overlaps with TH+ synaptosomes that do not contain any B represent the level of POI at DA axons. POI in B+ synaptosomes that do not contain any TH is representing the level of POI at active zones outside of subset of DA neurons. The bottom panel of Figure 9 shows the POI in any B+ synaptosomes, thus B that might or might not contain also TH. This condition is indicating how much POI is present at active zones regarding all subsets of neurons. In reverse, when TH+ synaptosomes contain POI independent of the presence of B, it is the representation of the amount of POI in DA neurons independent whether at release terminals or axons. The analysis of protein composition in ChI was carried out in a simplified way where only the bottom panel of Figure 9 is representing the ROIs. However, with different antibody combinations.

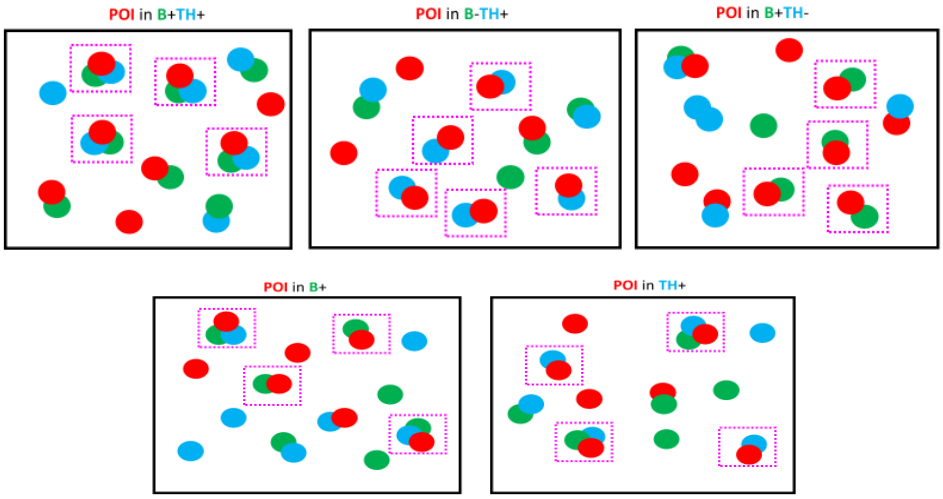


**Figure 9: Synaptosomes analysed in five different conditions.**

Different types of synaptosomes are colour coded. Red - protein of interest (POI), blue- marker of subset of neurons, in this case marker of DA neurons - enzyme tyrosine hydroxylase (TH), green - the active zone marker bassoon (B). Overlap condition of POI in B+TH+ is the illustration of level of POI at active zones in DA neurons. POI in B-TH+ is indicating the level of POI at DA axons. The level of POI in B+TH- is determining the level of POI at active zone outside of DA neurons. Bottom figure panel is representing the level of POI at active zones of all subsets of neurons (POI in B+) and the level of POI in DA neurons independent of the presence of active zone (POI in TH+). Source: author's chart.

### 2.5.2 Identification of regions of interest

A custom written MATLAB (The Mathworks Inc.) code was employed for the determination of overlapping patterns between different combination of proteins. For the analysis in dopaminergic neurons, subset of DA neurons was labelled with antibody against TH, enzyme responsible for DA synthesis and active zone marker bassoon, and POI. Analytical steps detecting the level of protein expression in ChI were carried out by identifications of ChI with the anti-vesicular acetylcholine transporter (vAChT) antibody and active zone markers bassoon, ELKS2 and postsynaptic density marker PSD95. The level of active zone protein in subtypes of neurons releasing classical neurotrasmitters glutamate and GABA was detected with the synaptosome imunolabelled using markers of their respective vesicular transporter proteins: vesicular GABA transporter (vGAT) and vesicular glutamate transporter (vGluT1).

### 2.5.3 MATLAB facilitated analysis of synaptosomes labelling cholinergic interneurons

Analytical processing in MATLAB was chosen, as running simplified script in NIH ImageJ software did not prove to be sufficient. Sript in ImageJ was applying the threshold cutoff only to one image channel, whereas graphical user interface of MATLAB allowed to input multiple selection factors such as shape aspect, number and size of pixels, intensity cutoff simultaneously for each inputted image channel.

#### 2.5.3.1 Generation of masked images including protein of interest

In case of analytical procedure for ChI, the inputted images were image channels including active zone and postsynaptic density markers (bassoon, ELKS2, PSD95) as channel corresponding to reference and markers of subsets of investigated neurons (vAChT, vGluT1, vGAT) as a reference. In separate experimental set, imunolabelling of active zone markers was replaced with labelling of vesicular markers exclusively. Synaptophysin - protein present as an integral part of synaptic vesicles - was used as channel corresponding to reference and markers of investigated subsets of neurons were again inputted as reference. Output of the

script represented detected values of intensities and overlapped percentages of the selected ROIs. Intensities were plotted in the form of frequency distribution histograms and profile plots that were used as supporting material for the assesment of SNR and quality control of the acquired confocal images.

### 2.5.4 MATLAB facilitated analysis of synaptosomes labelling dopamine neurons

The custom written script was run in sequential two-step analytical analysis (Table 4). Analysis of striatal synaptosomes labelling dopaminergic neurons was carried out in similar manner as the analysis of protein composition in ChI. At the initial stage of the quantitative process, simple overlaps were created where POI was chosen as channel corresponding to reference and image channels of TH+, and B+ synaptosomes respectively were inputted as reference. In case of testing accompanied by detection of protein levels in KO mice, analytical parameters based on wildtype (WT) synaptosome images were kept the same across both genotypes. The frequency distribution in histograms, profile plots and significant decrease between KO and WT control mice were evaluated before further quantitative processing. Generation of simple image channel overlaps represented a final step in the analysis of ChI protein composition, whereas it was an intermediate step in the analysis of dopaminergic neurons. Thereby, in the subsequent steps, combined overlapped objects composed of all three image channels were created.

#### 2.5.4.1 Generation of masked images without the protein of interest

Three different types of combined overlaps were generated (Table 4). For this purpose, the analytical procedure was carried out in two separate steps. In the first step, marker B was chosen as reference and TH as corresponding channel. Choosing a specific channel as reference resulted in selection of ROIs based on that particular image channel. The threshold cutoff was applied to both of them but the ROIs were selected based on reference only. This step was subsequently repeateded in reversed way when TH was chosen as reference and B was the corresponding channel. These steps resulted into generation of three types of masked images that used for the incorporation of the POI in the second step.

#### 2.5.4.2 Incorporation of test protein into generated masked images

For the generation of overlaps of POI and B+TH+ synaptosomes, masked images outputted from the first step were defining the ROIs, thus were inputted as references and POI represented the corresponding channel. However, when progressing to generation of negative overlaps, the image subtraction was necessary in between the first and second round of MATLAB analysis. Subtraction was carried out using NIH ImageJ software. Output of the first step resulted in generation of two categories of images within the same type of overlap, namely masked overlapped and selfmasked images of the individual image channels. During the subtraction selfmasked images were subtracted form masked overlapped images. The subtracted images were ready to be inputted as reference channel leading to final quantitative results.

**Table 4: Synaptosome MATLAB analysis.**

Steps for quantitative analysis of protein levels at dopaminergic synaptosomes are shown. Analysis of protein levels in ChI is comprising the processing as shown in simple overlapped objects with different combination of antibodies, thus with different combination of markers. When both markers (B; TH) were considered positive, no sutraction was necessary. In contrast, when one of the markers was negative, subtraction of selfmasked from overlapped images was undertaken. Second step incorporates the POI leading to final outcome. Source: author's chart.

| 1st step | | | | 2nd step | |
|---|---|---|---|---|---|
| Combination of image channels | Reference channel | Corresponding channel | Image subtraction | Reference channel | Corresponding channel |
| **Simple overlapped objects** | | | | | |
| **POI B+** | B | POI | --- | --- | --- |
| **POI TH+** | TH | POI | --- | --- | --- |
| **Combined overlapped objects** | | | | | |
| **POI B+ TH+** | B | TH | --- | B+ TH+ | POI |
| **POI B- TH+** | TH | B | selfmasked TH - overlapped TH+ B+ | B- TH+ | POI |
| **POI B+ TH-** | B | TH | selfmasked B - overlapped B+ TH+ | B+ TH- | POI |

POI – protein of interest, B – bassoon, TH – tyrosine hydroxylase

### 2.5.5 Statistical analyses

Statistical analyses were carried out in Prism (GraphPad). Mann-Whitney rank sum test was used in Figures 12, 16, 19. Kruskal-Wallis analysis of variance with post hoc Dunn's test was used in Figures 11A, 21A, 22A, 23A, and 24A. Significance was set as * $p<0.05$, ** $p<0.01$, and *** $p<0.001$ for all data. Image acquisition of synaptosomes prepared from different genotypes was performed as blinded experiments. Quantitative parameters were based on WT confocal images and were set equally for both genotypes.

### 2.5.6 Miscellaneous

All chemicals were of the highest available purity and were purchased from standard sources. All animal experiments were conducted in accordance with the guidelines of the Harvard University Animal Care and Use Committee.

# 3 Results

## 3.1 Experimental quality assurance and control

Experimental quality for the quantitative purposes was assessed at multiple levels. Quality of the synaptosome preparation was determined by non-quantitative chemiluminescent western blots from intermediate and the final biochemical fractions (Figure 10). Furthermore, proteins with the known level of expression were tested in parallel with the new POI confirming the quality of synaptosome preparation. Used antibodies have verifying KO or knock-down (KD) based records from previous studies or respective manufacturer tests. However, the accessibility of antigen-antibody binding site and the homogeneity and thus the penetrability of synaptosome sample might significantly differ from other types of samples. Thereby, background staining and verification of antibody were directly tested by comparison of detected levels in KO mice. The experiment was also viewed in a form of frequency distributions of individual ROIs within each experiment in histograms and profile plots.

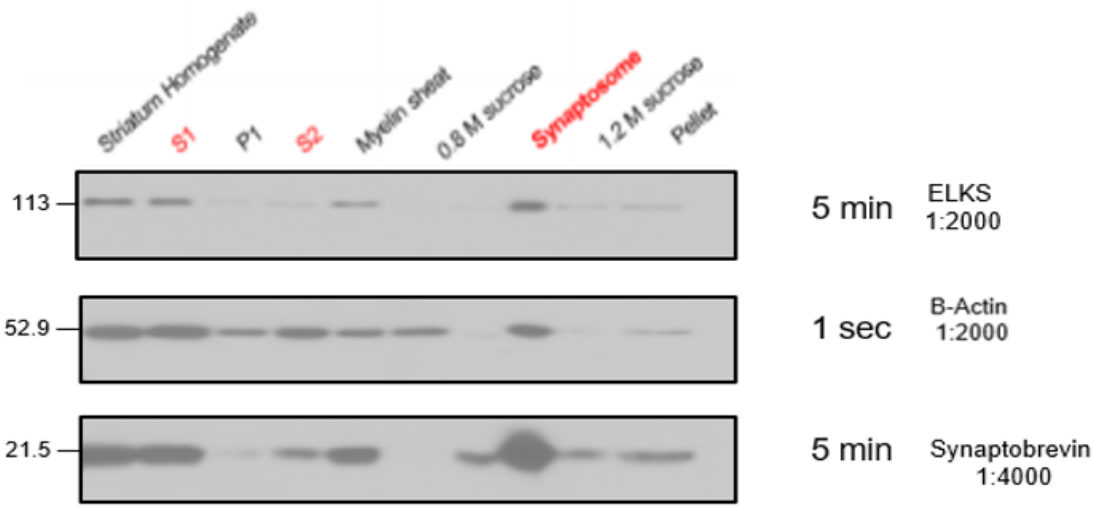


**Figure 10: Western blot of synaptosome and intermediate step biochemical fractions.**

Synaptosomes and fractions obtained during intermediate steps of preparation are shown in enriched form with vesicular marker synaptophysin, loading control in a form of cytoskeletal protein B-actin and active zone protein ELKS. Red colour indicates fractions that were taken for further processing. The pellet was snap frozen in dry ice and re-homogenized. The exposure time, molecular weight in kDA and antibody dilutions are indicated. Source: author's chart.

## 3.2 Determination of protein composition in dopamine neurons

### 3.2.1 Clusters of protein assembly bassoon, ELKS and RIM

Liu *et. al* has shown that DA varicosities are composed of sparsely distributed assemblies of active zone proteins bassoon, RIM and ELKS mediating action potential triggered DA release. Prior continuing with testing the presence of other active zone proteins, previously generated datasets were reproduced. The specific focus was directed on central organizer of active zones - protein RIM, mediator of priming of synaptic vesicle - Munc13s, protein involved in membrane trafficking - ELKS2, and negative control DAT. Previously applied quantitative analysis through NIH ImageJ software has been optimized and transformed into custom written MATLAB code.

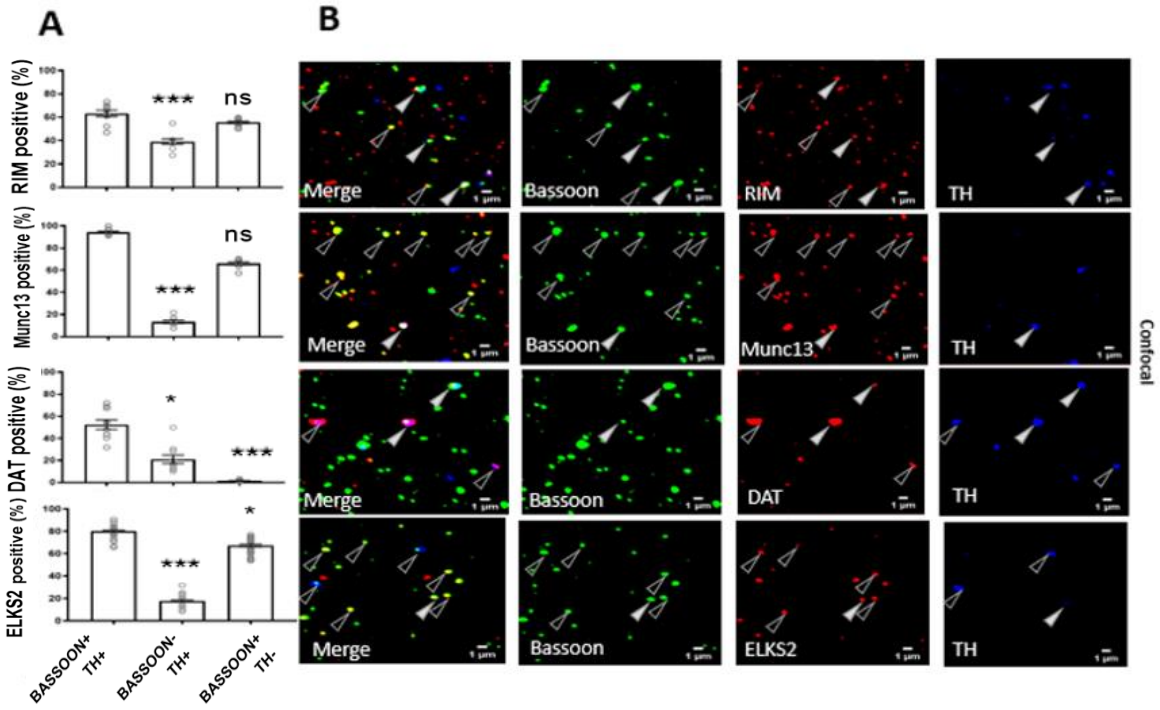


**Figure 11: Positive and negative controls.**

Quantitative results of MATLAB facilitated analysis reproducing the results of Liu *et. al.* Synaptosomes in three conditions: B+TH+, B-TH+ and B+TH- respectively. Negative control DAT shows levels approaching zero outside DA neurons (A). Confocal images of synaptosomes. Filled arrowheads indicate colocalization between all three components, hollow arrowheads indicate colocalization of two components (B). Each circle represents the average result of an area with 200-900 synaptosomes. n= 30 areas/ 3 mice for bassoon positive, 10/1 for Munc13, DAT, and RIM positive. All data are expressed as means ± SEM. ***p<0.001; *p<0.05, ns, not significant. Kruskal-Wallis analysis of variance with post hoc Dunn's test. Source: author's chart.

### 3.2.2 Liprin-α3

Liprin-α3 is a scaffolding protein and a binding partner of proteins ELKS, RIM, rho effector protein, β-Liprins and binding partner to itself resulting in homodimer formation. The structure is composed of two Liprin homology domains at the N-terminus and three sterile alpha motifs (SAM) at the C-terminus. Only isoforms Liprin-α2 and α3 are expressed in the brain (Serra-Pages, Medley, Tang, Hart, & Streuli, 1998; Spangler et al., 2011; Sudhof, 2012). Previous studies show its role and localization at hippocampal synapses (Wong et al., 2018). However, its presence at synapses of DA neurons in the striatum has remained unknown.

### 3.2.3 The level of expression of Liprin-α3 in dopamine neurons

Using constitutive KO mice for Liprin-α3 together with WT controls, it was established that Liprin-α3 is present at DA release sites as determined by normalized quantification of fluorescent intensity of Liprin-α3+ synaptosome that contain the marker of active zones - protein bassoon, as well as marker of DA neurons - enzyme TH (Figure 12). However, the significant decrease between genotypes was detected also at DA axons as determined by Liprin-α3+ synaptosomes that contain enzyme TH but do not contain any protein bassoon. These finding are also supported with high level of RNA in the investigated brain region as determined by microarray and *in situ* hybridization experiments (Figure 2, Figure 3). However, difference in expression between these two conditions cannot be objectively stated due to analytical limitations. The analysis based on quantifying overlap percentage between the markers and POI could not be employed due to shape properties of Liprin proteins. The findings are therefore based on the quantified and normalized intensity values. The preclusion of intensity-based quantification is the dependence on the size of the area. Since the size of the area is different with every overlap condition, it cannot be objectively compared across. The resolution of confocal microscope does not allow precise nanoscale determination of the area per synaptosome, whereas the enhancement using supperresolution significantly reduces the number of synaptosome per image. It would not provide optimal sample size for quantitative purposes.

All experiments were pursued with the experimenter blind to genotype until final quantitative step. The imaging was obtained with identical acquisition paraments. The quantitative parameters were determined based on WT controls.

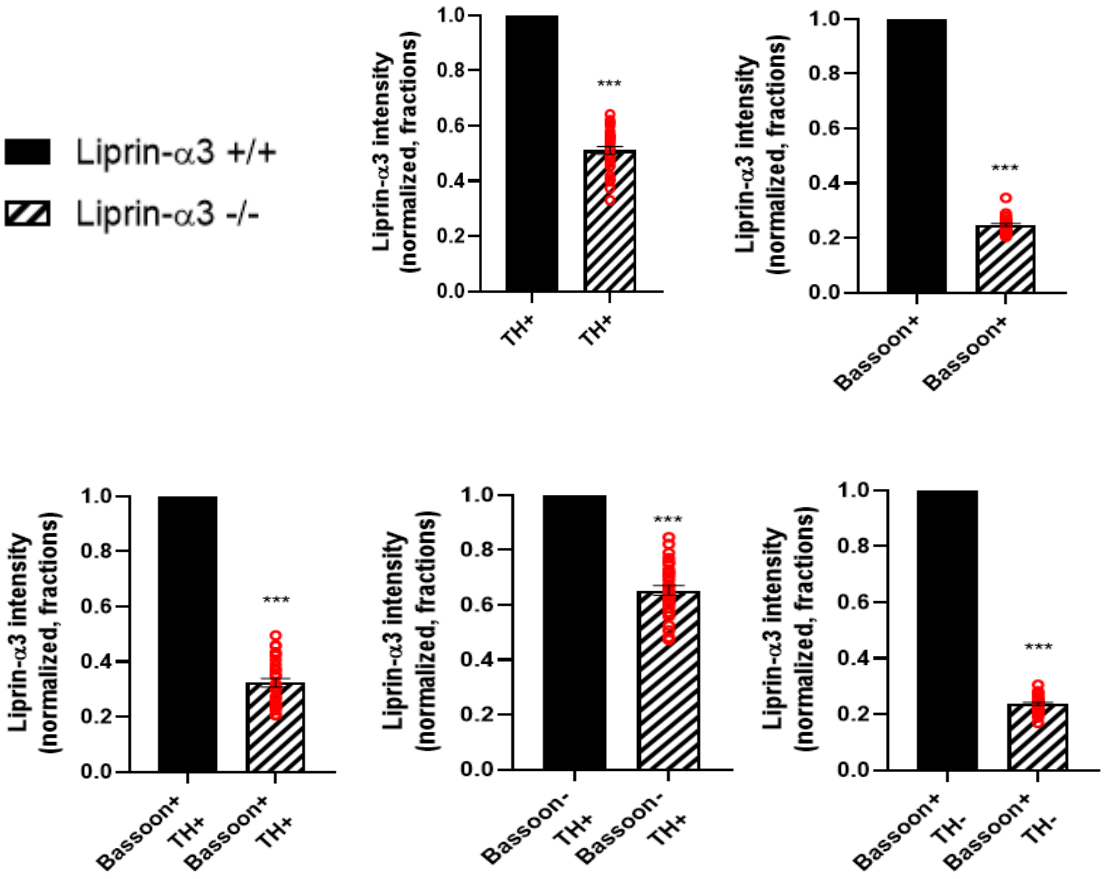


**Figure 12: Detected levels of Liprin-α3 in WT and constitutive KO mice.**

Intensities were normalized to respective WT controls. The KO represents a background level. Decrease in TH+ ROIs both, at active zones and at DA axons is revealing the presence of Liprin-α3. Each circle represents the average result of an area with 200-900 synaptosomes. n= 29 areas/3 mice for Liprin-α3 +/+, 30/3 for Liprin-α3 -/-. All data are expessed as means ± SEM. ***p < 0.001; Mann-Whitney test. Source: author's chart.

Fluorescent staining revealed apparent decrease in number of Liprin-α3+ synaptosomes in Liprin-α3 -/-, as the protein is knocked out in global level. The cross-reactivity of the used antibody was verified in previous studies (Wong et al., 2018), the antibody is cross-reacting only with non-brain isoforms of Liprin proteins. Liprin-α3 has a less distinct shape than other active zone proteins, has a broader distribution with antibody staining spread throughout the nerve terminal (Figure 13).

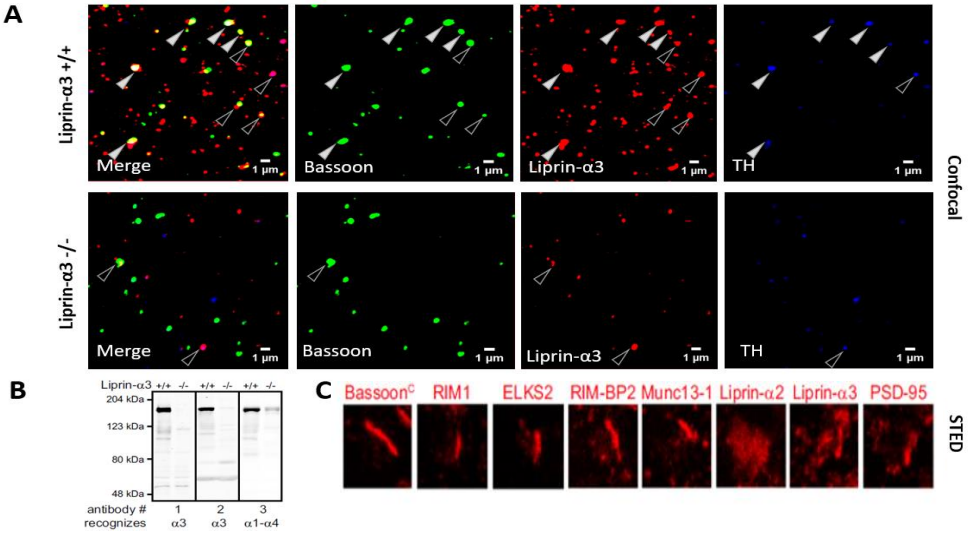


**Figure 13: Liprin-α3 positive synaptosomes.**

Confocal images of Liprin-α3 +/+ and Liprin-α3 -/- demonstrating the colocalization between bassoon and TH. Filled arrowheads indicate colocalization between all three components, hollow arrowheads indicate colocalization of two components (A).The level of antibody crossreactivity was verified (Wong et al., 2018), crossreactivity with non-brain isoforms does not effect these experiments (B). Shape of Liprin-α proteins shown in superresolution images (C). Experiments were pursued with experimenter blind to genotype and identical acquisition parameters set. Source of figures B, C modified after (Wong et al., 2018).

Histograms of selected ROIs show shift towards bins with smaller intensity values in case of KO mice and higher frequency of values at bin with greater intensities in case of WT controls. This view verifies the chosen ROI, as false positives or overall insufficient experimental quality would be ultimately reflected by frequency distributions. Profiles are depicted as absolute values in arbitrary units (AU), (Figure 14).

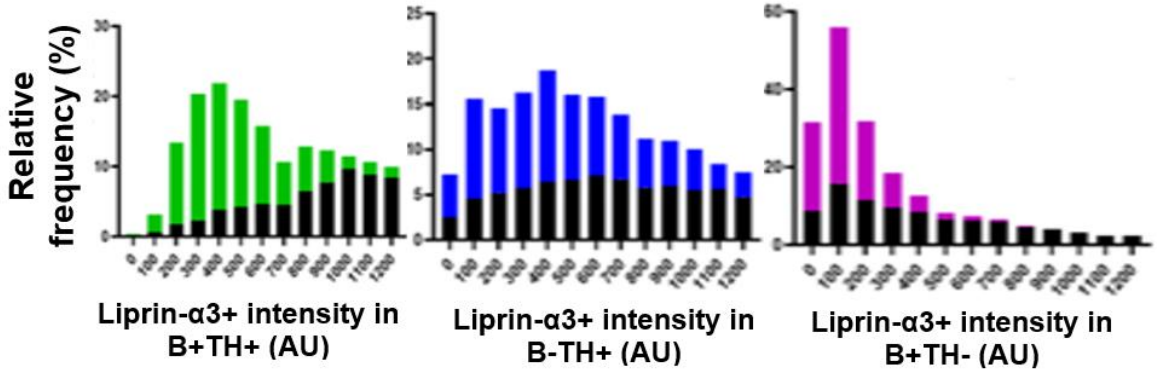


**Figure 14: Relative frequency distribution of Liprin-α3 intensities in defined ROIs.**

Liprin-α3 relative frequency; KO (color), WT (black). Absolute intensity values expressed in arbitrary units (AU). n=~1 000 ROIs/ 1 mouse for Liprin-α3 +/+ and ~400/1 for Liprin-α3 -/-. Source: author's chart.

### 3.2.4 Liprin-α2

Together with Liprin-α3 belongs to only isoforms of Liprin-α proteins expressed in the brain. Previous studies have supporting evidence for its localization associated with presynaptic terminal. As well as, synaptic transmission was shown to be impaired upon the removal of this protein isoform (Spangler et al., 2011; Spangler et al., 2013; Zurner, Mittelstaedt, tom Dieck, Becker, & Schoch, 2011).

### 3.2.5 The level of expression of Liprin-α2 in dopamine neurons

To address the question whether Liprin-α2 is expressed at DA release sites and DA axons, conditional KO mice and control WT mice were tested. Liprin-α2 was specifically removed only from subset of DA neurons using Cre recombination. Decrease in TH+ ROI followed the expected outcomes. However, detected significant decrease in bassoon cannot be correlated to a supporting reasoning. As the protein KO was restricted to only 3% of DA neurons that accounts for the number of DA axons in the striatum, the level of decrease should not be changed in the global level. Further analytical restriction of tested conditions, namely to detection of the level in active zone at DA neurons minimized the decrease (Figure 16). This might reflect improper ROI selection during quantitative step which might be the consequence of insufficient experimental quality and/or SNR of acquired images. However, contributing factor is accounting for finding of previous studies that Liprin-α2 is strongly localized to active zone only upon removal of Liprin-α3 (Wong et al., 2018). Thus, this approach might not be optimal for the answering of this research question. Testing in Liprin-α2,3 double KO would provide insights, however, for this purpose, the specificity of used antibody has to be demonstrated.

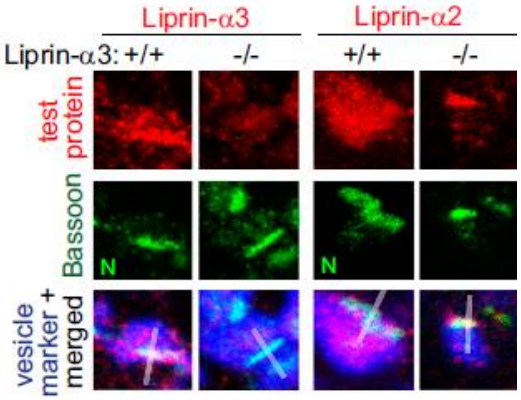


**Figure 15: Localization of Liprin-α2 to active zone.**

Liprin-α2 is w idespread throughout the nerve terminal in WT animals. It is trasnslocated to active zone upon removal of Liprin-α3 as determined under superresolution microscopy colocalizing with active zone marker bassoon. Source reffering to: (Wong et al., 2018).

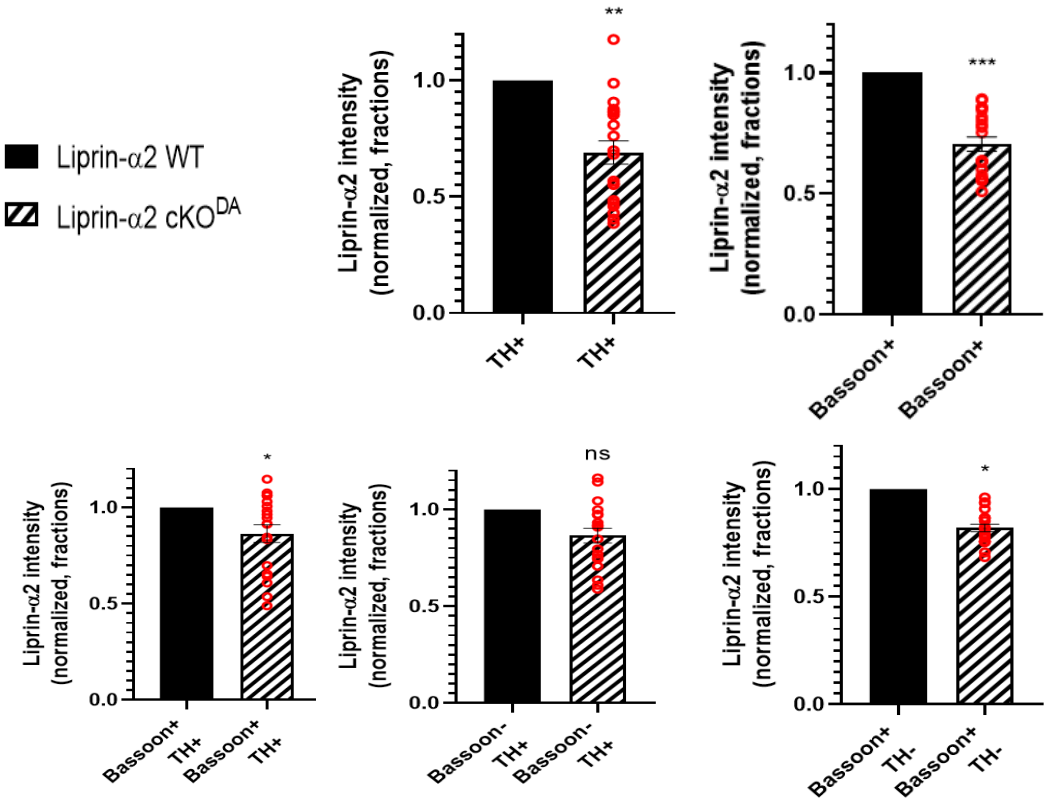


**Figure 16: Detected levels of Liprin-α2 in WT and conditional KO mice.**

Detected decrease at active zones in global level do not support the outcomes of proper ROI selection, thus does not provide clear interpretation. Each circle represents the average result of an area with 200-900 synaptosomes. n= 20 areas/2 mice for Liprin-α2 WT, 20/2 for Liprin-α2 cKO$^{DA}$. All data are expessed as means ± SEM. ***p<0.001; **p< 0.01; *p<0.05; ns, not significant. Mann-Whitney test. Source: author's chart.

The histograms indicate different frequency distribution than for Liprin-α3, as the protein is KO only from a subset of DA neurons accounting only to 3%. Shift towards higher WT values can be found only at histograms including TH+ synaptosomes.

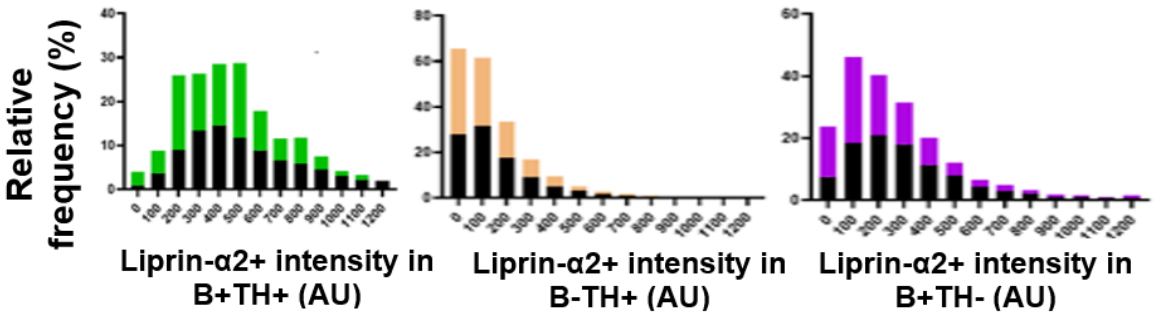


**Figure 17: Relative frequency distribution of Liprin-α2 intensities in defined ROIs.**

Liprin-α2 relative frequency; cKO$^{DA}$ (color) WT (black). Absolute values expressed in arbitrary units (AU). n=~1000 ROIs/ 1 mouse for Liprin-α2 WT, ~1000/1 for Liprin-α2 cKO$^{DA}$. Source: author's chart.

Profile plots represent the function of the strength of the signal, as well as the SNR depicted as intensity of grey-value to distance from the midpoint on the line drawn through the centre of synaptosome. For antibodies with better binding properties such as anti-bassoon, the area under the curve with greater intensity value is wider. Straight line is the reflection of multiple pixels depositing the same intensity values (Figure 18A). It is establishing indirect estimation, as the selected synaptosome, as well as crossing the line are determined by the experimenter.

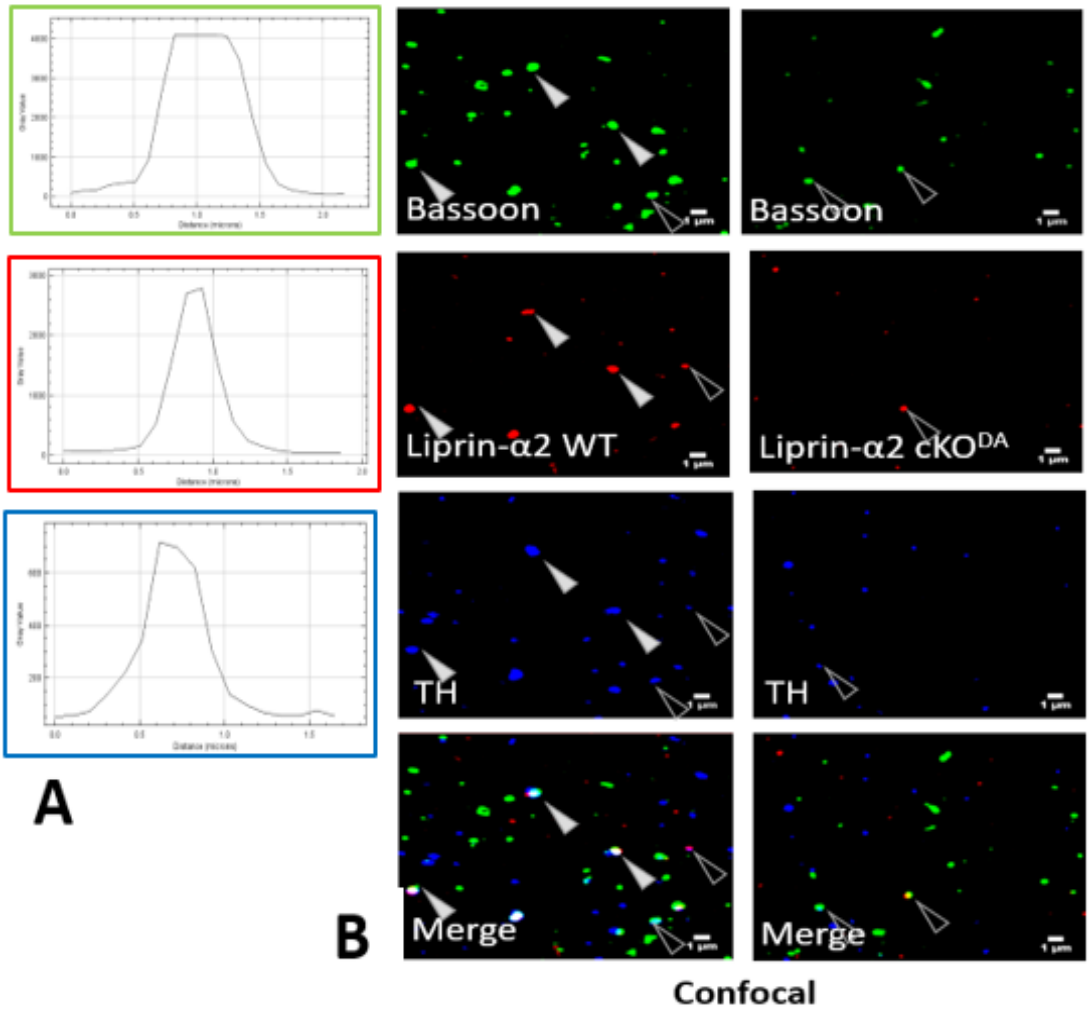


**Figure 18: Liprin-α2 positive synaptosomes.**

Profile plots of signal intensity distribution within single synaptosome (A). Confocal images of synaptosomes. Number of Liprin-α2+ synaptosome should be similar across genotypes, however, images of cKO control quantified from these experiments indicate firm decrease. Experiments were pursued with experimenter blind to genotype and identical acquisition parameters set (B). Source: author's chart.

### 3.2.6 Changes in levels of RIM upon Liprin-α3 removal

Testing the change in RIM levels upon the removal of Liprin-α3 has indicated no change except when bassoon was restricted as ROI. This might reflect a consequence of release site rearrangement rather than RIM decrease itself. Upon removal of Liprin-α3, position of bassoon changes (Wong et al., 2018). In that case ROIs based on bassoon in WT mice would not be complementary with ROI from KO animals. It correlates with findings of Wong *et. al* where bassoon peak intensity increased for N-terminus and decreased for C-terminal end (Figure 20C).

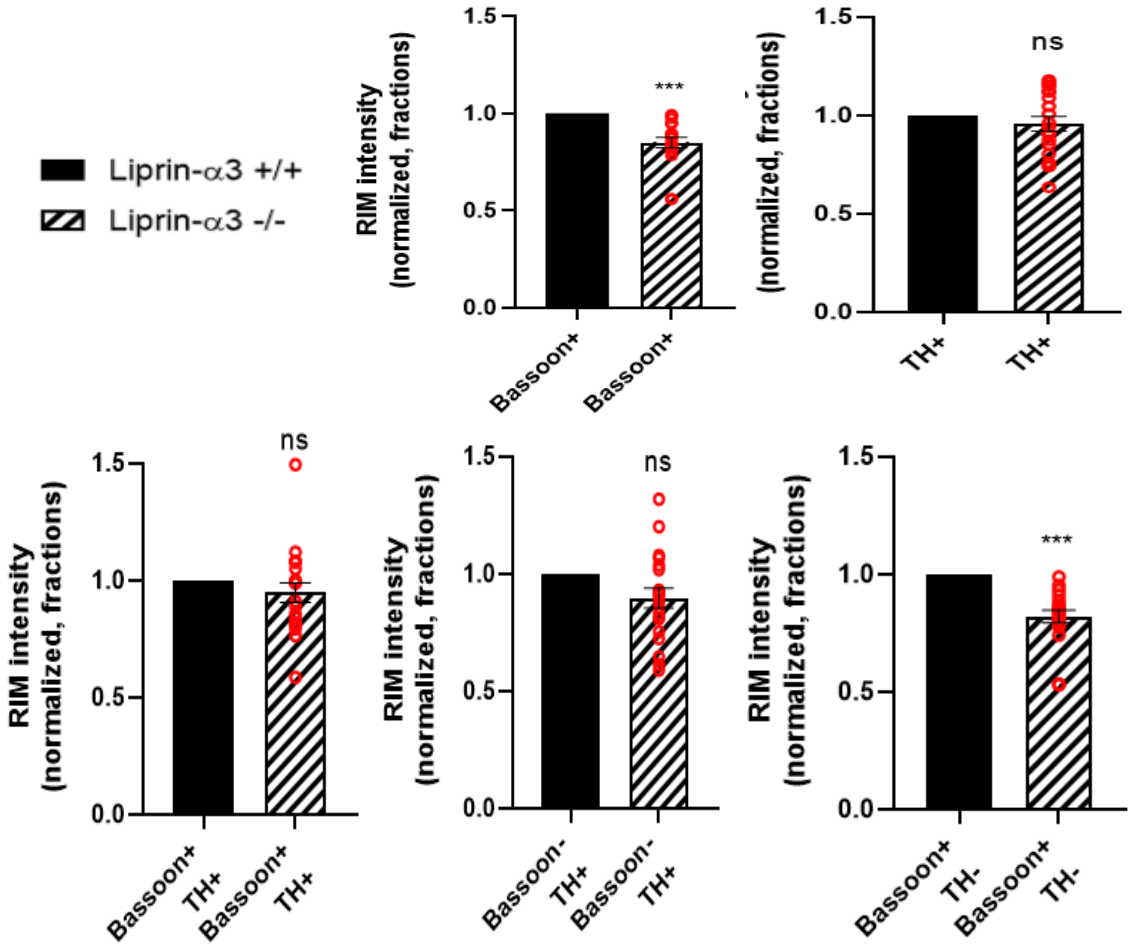


**Figure 19: Detected changes in RIM levels.**

Detected no change of RIM levels outside of active zones. Each circle represents the average result of an area with 200-900 synaptosomes. n= 20 areas/2 mice for Liprin-α3 +/+, 20/2 for Liprin-α3 -/-. All data are expessed as means ± SEM. ***p<0.001; ns,not significant. Mann-Whitney test. Source: author's chart.

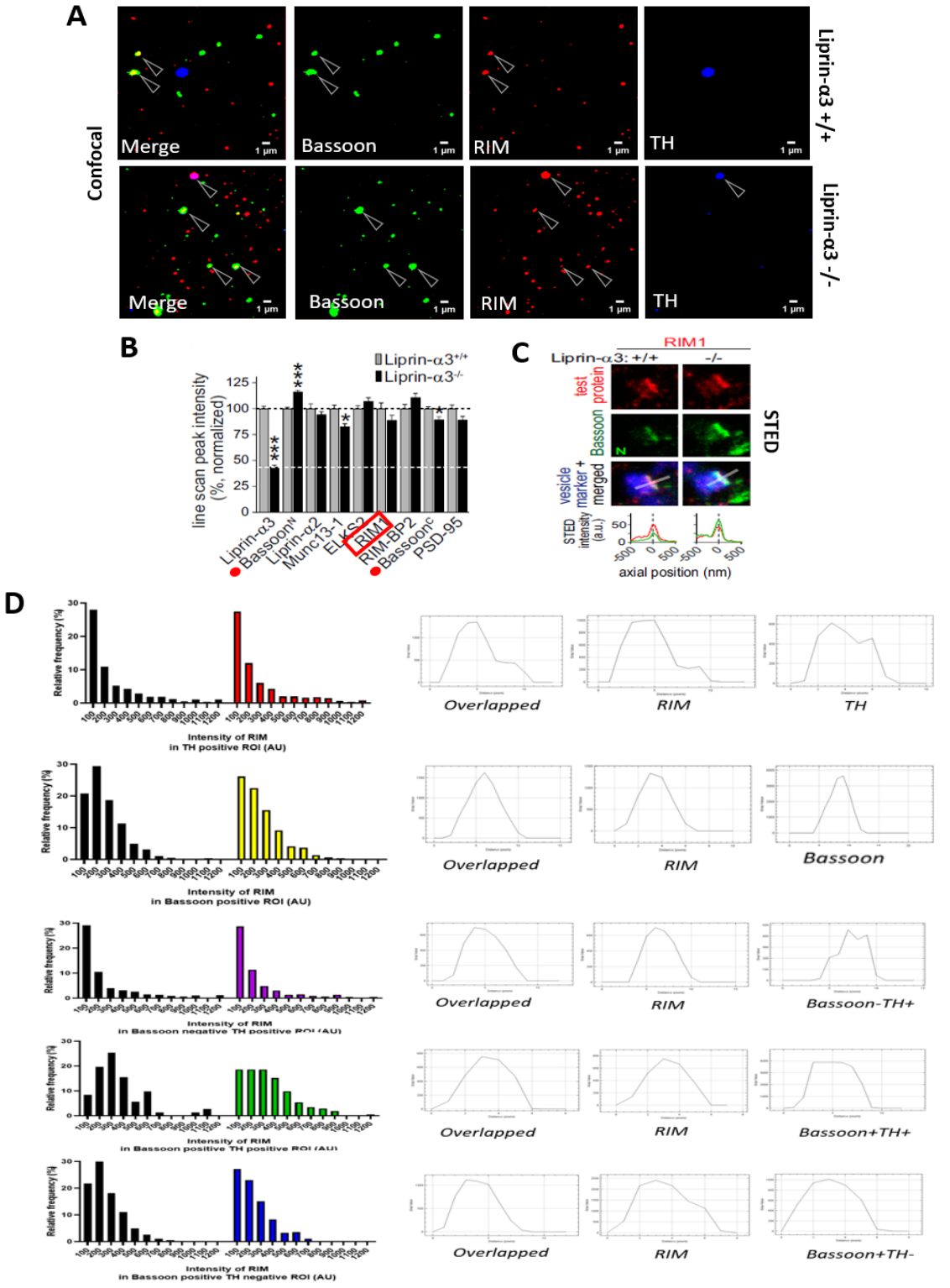


**Figure 20: RIM immunostaining in Liprin-α3 constitutive KO.**

Confocal images of synaptosomes. Experiments blind to genotype with identical acquisition parameters set (A). Peak intensities for RIM, bassoon and other active zone proteins in Liprin-α3 -/- under superresolution (B,C). Histogram and profile plots of individual ROIs; Liprin-α3 +/+ (black), Liprin-α3 -/- (colour), (D). Source of figures B,C modified after: (Wong et al., 2018).

### 3.2.7 ELKS1, piccolo and synaptotagmin1

Further tested proteins comprised binding partner of Liprin-α proteins - ELKS1, as well as bassoon homolog - piccolo that is characterized with proline and glycine residues that prevent folding. From 15 isoforms of synaptic protein synaptotagmin, isoform synaptotagmin1 present on synaptic vesicles was tested (Sudhof, 2012).

### 3.2.8 Wildtype based level of expression of ELKS1, piccolo and synaptotagmin1

Preliminary data suggest that these proteins are expressed at DA release sites and at active zones of other subsets of neurons, expressed to a smaller extent at DA axons. Properties of used antibodies were confirmed in previous KO/KD tests; however, further control experiments need to better establish these findings. Resulting from the shape of tested proteins, quantification is based on percentual overlap between markers and POI, thus also allows objective comparison across conditions.

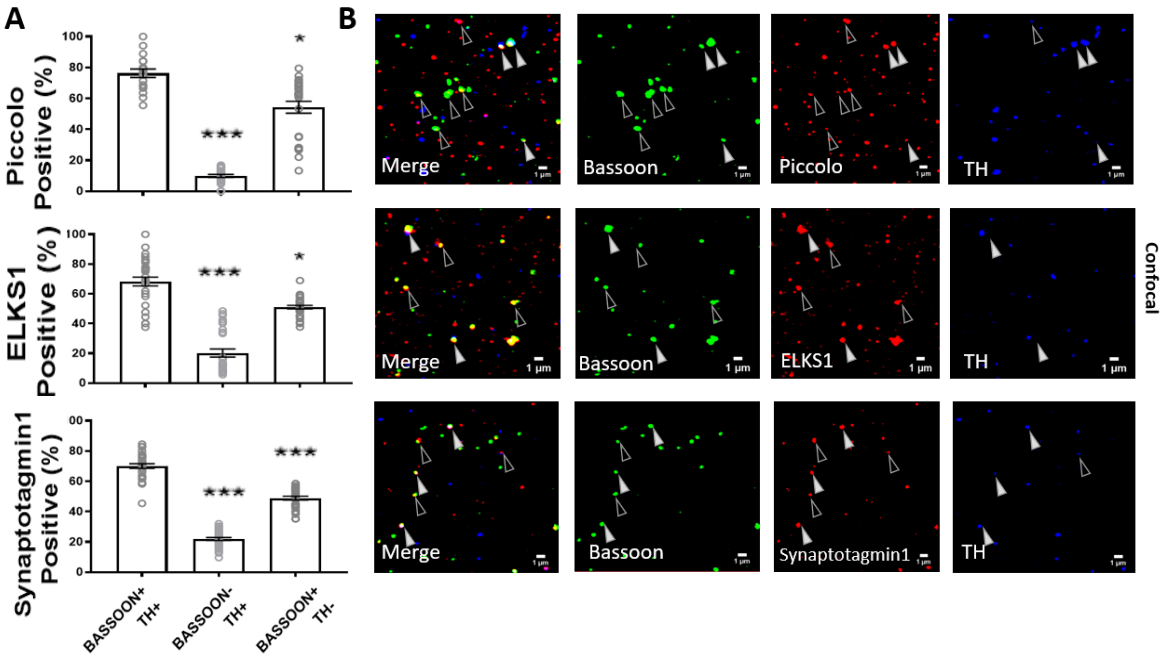


**Figure 21: Proteins tested in wildtype animals.**

Percentage of POI positive synaptosomes at active zones in DA neurons, DA axons, active zones of other subsets of neurons, respectively (A). Representation of confocal images used for quantification (B). Each circle represents the average result of an area with 200-900 synaptosomes. n=30 areas/3 mice. All data are expessed as means ± SEM. ***p<0.001; *p<0.05. Kruskal-Wallis analysis of variance with post hoc Dunn's test. Source: author's chart.

### 3.2.9 RIM-BPs

RIM-binding protein – large multidomain protein and a linker between $Ca^{2+}$ channels and RIM protein (Acuna, Liu, Gonzalez, & Sudhof, 2015; Sudhof, 2012). It was tested in double cKO mice lacking isoforms RIM-BP1 and RIM-BP2 specifically in DA neurons. However, obtained results do not allow clear interpretation, as the decrease between WT and $cKO^{DA}$ mice does not show statistical significance. Properties of the used antibody were verified in previous studies (Wang et al., 2016). However, this demonstration relates to this experimental set-up only to a partial extent, since these outcomes might not correlate with the antibody binding properties administrated in synaptosomes. The used analytical method does not allow classification of obtained results into positive and negative regarding the presence of the POI. Detected levels do not confirm the presence of this protein, however, whether it is because of its missing presence or insufficiency of any of the experimental steps, stays an open question. These outcomes do not indicate the presence of RIM-BP2 at DA release sites but simultaneously do not exclude its missing expression.

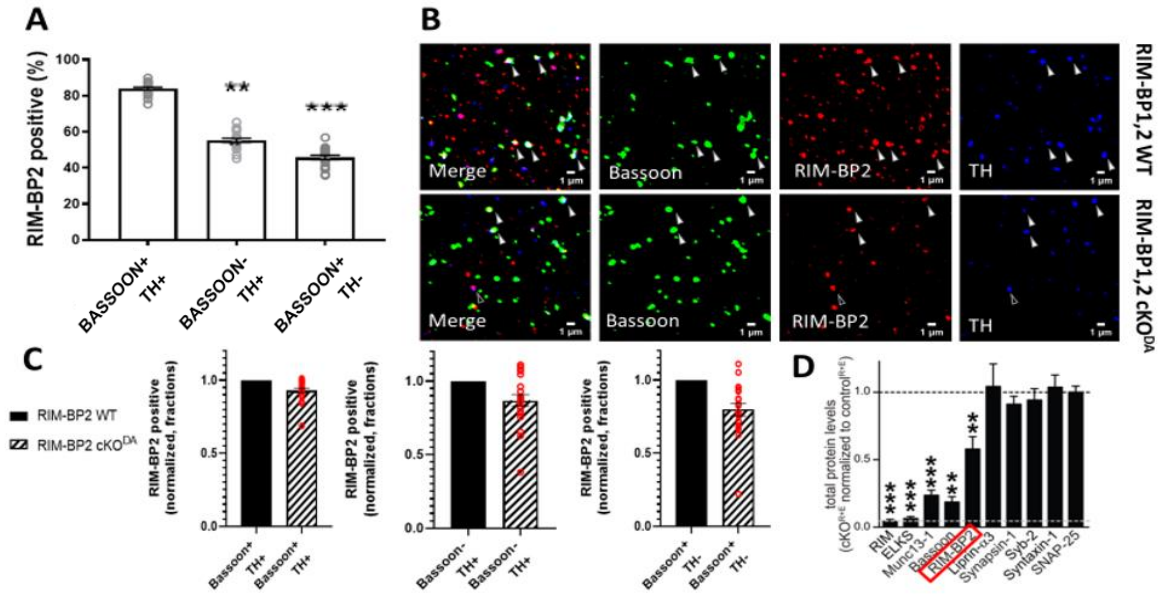


**Figure 22: Summary of assessment of the level of RIM-BP at dopamine release sites.**

Quantification of RIM-BP2 positive synaptosomes (A) and confocal images (B). Kruskal-Wallis analysis of variance with post hoc Dunn's test. Each circle represents the average result of an area with 200-900 synaptosomes. n= 20 images/2 mice for RIM-BP1,2 WT, 20/2 for RIM-BP1,2 $cKO^{DA}$. Comparison of detected levels between genotypes (C). Antibody verification in RIM and ELKS double cKO. Source of figure D modified after: (Wang et al., 2016).

## 3.3 Determination of protein composition in cholinergic neurons

Cholinergic inputs trigger DA release (Cachope & Cheer, 2014; Threlfell et al., 2012). However, the presence of specialized release sites in this subset of neurons has not been determined before. Applying methodology used for the determination of protein levels in dopaminergic neurons, the level of active zone proteins in ChI have been addressed. Cholinergic interneurons were identified with the presence of vesicular transporter vAChT. Active zone proteins bassoon and ELKS with previously established level in dopaminergic neurons have been tested the first.

### 3.3.1 Molecular scaffold bassoon and ELKS in cholinergic neurons

Active zones were labelled with fluorescent antibody recognizing protein bassoon that is guiding synaptic vesicles to release sites. Colocalization between bassoon and the marker of subset of ChI have been determined in <20% vAChT+ synaptosomes. Classical neurotransmitters such as glutamate and GABA require specialized release sites for coupling of $Ca^{2+}$ to vesicle fusion. Outcomes were compared with percentual overlap levels between active zone markers and GABAergic, glutamatergic neurons as identified by respective vesicular transporters (vGAT, vGluT1). Detected level has resulted in 3-4-fold increase between active zones present in ChI and neurons releasing classical neurotransmitters. The absolute value might underestimate the representation of actual biological percentage, as the criteria for analysis were restricted mainly to synaptosomes governing the most adequate characteristics. However, the relative rather than absolute percentage between these subsets of neurons is providing the basis for interpretation. Colocalization of postsynaptic density have been tested as a follow-up (Figure 23). However, as higher molecular weight of postsynaptic membrane might not allow it to sustain homogenization, the absolute number of PSD95 might be in overall lower limiting the sample size. Histograms convey the relative intensity distribution of selected active zone proteins in quantified ROIs based on respective vesicular markers. The highest frequency of bassoon, ELKS or PSD95 positive is in majority in bins with the smallest value within vAChT ROIs. Intensity distribution confirms the low detected level of active zone proteins.

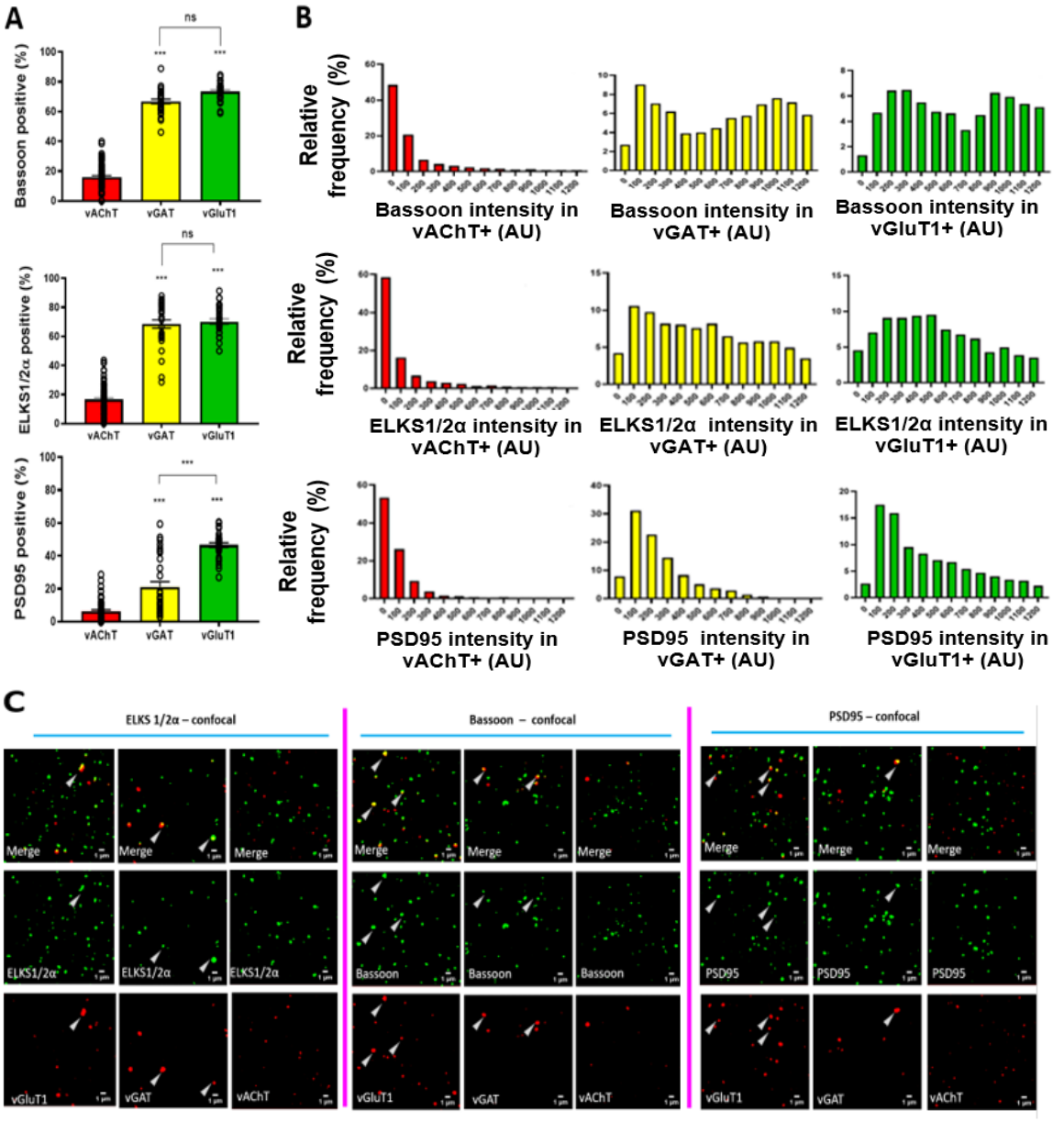


**Figure 23: Low level of active zone proteins in cholinergic neurons.**

Quantification of the percentage overlap of synaptosomes that contain bassoon, ELKS1/2α and PSD95 respectively in three different subsets of neurons identified by their respective vesicular markers (A). Histograms of quantified POI intensities in defined ROIs shown as the percentage of relative frequency to intensity value displayed in AU in bins. Histograms are colour matched with used types of vesicular markers (B). Representative confocal images of immunolabelled synaptosomes (C). Each circle represents the average result of an area with 200-900 synaptosomes. n=26 areas/ 3 mice for bassoon positive (%) in TH, 74/ 3 for bassoon positive (%) in vAChT, 29/4 for bassooon positive (%) in vGAT, 29/4 for bassoon positive (%) in vGluT. 28/3 for ELKS1/2α positive (%) in TH, 89/3 for ELKS1/2α positive (%) in vAChT, 30/ 3 for ELKS1/2 positive (%) in vGAT. 30/ 3 for ELKS1/2 positive (%) in vGluT1. All data are expessed as means ± SEM. ***p<0.001; ns, not significant. Kruskal-Wallis analysis of variance with post hoc Dunn's test. Source: author's chart.

### 3.3.2 Presence of synaptic vesicles in cholinergic synaptosomes

To confirm that structure of isolated synaptic terminals from ChI comprise characteristics of synaptosomes, the presence of synaptic vesicles was tested. Fluorescent antibodies against integral protein synaptophysin were used to determine the colocalization between this vesicular marker and respective vesicular transporters. For comparison, classical neurotransmitters with verified presence of synaptic vesicles were tested in parallel. Obtained results show the same level of synaptophysin positive synaptosomes that contain vAChT, as synaptosomes that contain vGAT (Figure 24A). The level of vGluT1 resulted in higher percentage. Quantitative studies of single vesicle proteins carried out in protease treated synaptosome support the level detected in vGAT and vGluT1 ROIs (Boyken et al., 2013; Mutch et al., 2011).

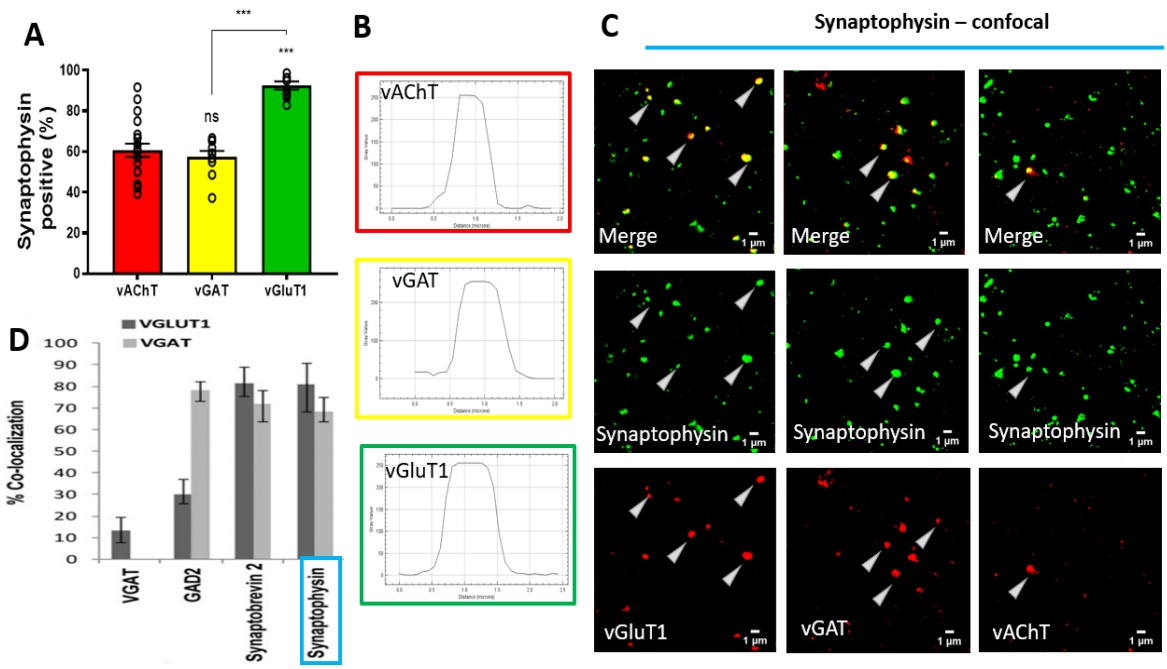


**Figure 24: Synaptophysin positive synaptosomes.**

Quantification of the percentage of synaptosomes that contain synaptophysin in three different subsets of neurons identified by their respective vesicular markers (A). Profile plots of quantfied ROIs shown as the grey-value intensity to distance from midpoint of line drawn throught synaptosome center (B). Representative confocal images of immunolabelled synaptosomes (C). Quantification of single vesicular proteins. (D). Each circle represents the average result of an area with 200-900 synaptosomes. n=10 areas/ 1 mouse. All data are expessed as means ± SEM. ***p<0.001; ns, not significant. Kruskal-Wallis analysis of variance with post hoc Dunn's test. Source of figure D modified after: (Mutch et al., 2011).

Higher level of synaptophysin on vesicles identified by vGluT1 might be due to monodispersity of vGluT1 on synaptic vesicles which contributes to even distribution, less likely occurrence of variation in the number of transporters per vesicles and better access to antibody-antigen binding site. In contrast, other transporters are polydispersed which accounts for frequent blocking of antibody binding site (Mutch et al., 2011). Used antibody has been tested to greater extent in transgenic mice expressing synaptophysin-tdTomato specifically in ChI. Colocalization between natural fluorescent signal of transgenic animal and used antibodies was assessed in brain slices and synaptosomes (Figure 25). As synaptosomes comprise much smaller area to observe the fluorescent signal, detected signal in synaptosomes was dim. For reliable assessment, the immunostaining was repeated in brain slices (20 um thick, Leica, VT1200s). Synaptophysin RNA level sequenced by previous microarray experiments suggests higher expression of synaptophysin in ChI than dopaminergic neurons, and previous studies in dopaminergic neurons detected signal of sufficient intensity (Liu et al., 2018). Fluorescent signal might be quenched upon fixation or genetic modification does not show same efficacy.

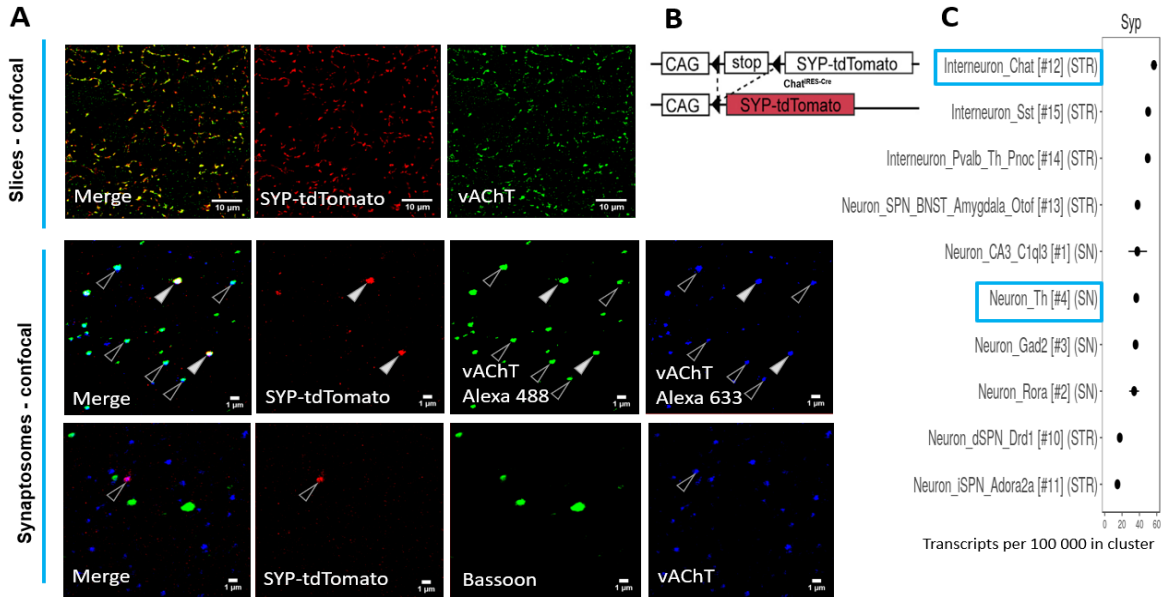


**Figure 25: Antibody verification in SYP-tdTomato expressing mice.**

Colocalization between signal from fluorescently tagged antibody and natural fluorescence of transgenic mice in confocal images of brain slices and synaptosomes (A). Vesicles in ChI were labeled by crossing Cre-dependent synaptophysin-tdTomato mice (SYP-tdTomato) with Chat$^{IRES-Cre}$ mice (B). RNA level from microarray experiments (C). Sources of figures B,C modified respectively after: (Liu et al., 2018); “DropViz”, http://dropviz.org/.

# 4 Discussion

## 4.1 Proteins present at dopamine release sites

Pursued experiments establish the presence of protein Liprin-α3 at DA release sites and in DA axons. Determining the difference in expression between these conditions requires supporting experiments or modified analytical method. Liprin-α proteins comprise different solubility properties resulting in less distinct shape than other active zone proteins. Approaching analysis based on determination of percentual overlap between selected markers of active zones and dopaminergic neurons, and POI would not objectively reflect the biological value. Originating from the properties of synaptosomes, global thresholding systems did not result in correct object recognition. Only quantitative analysis of intensity measurements, together with manual selection of thresholding values were proven to be effective. Outcomes are supported with constitutive KO controls, antibody with verified properties and the level of RNA expression of POI based on microarray and *in situ* hybridization experiments. Thus, the conclusion drawn from obtained data states that action potential triggered DA release is mediated by active zone proteins bassoon, ELKS, RIM and Liprin-α3.

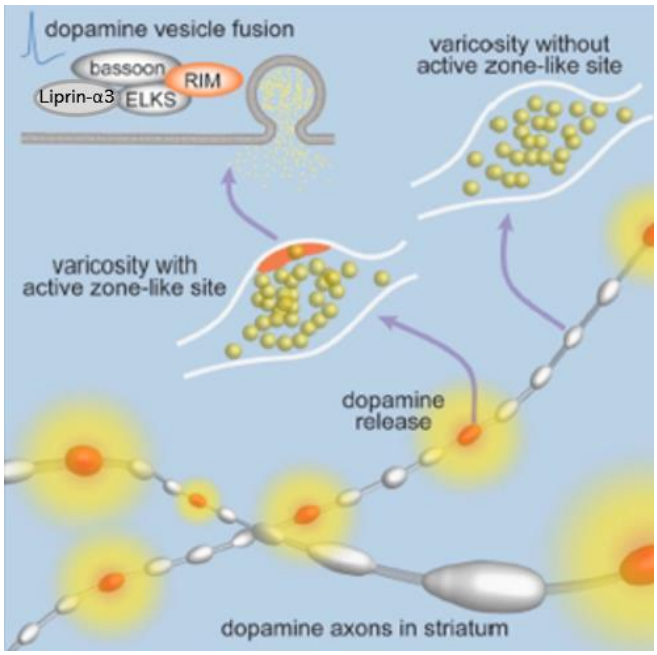


**Figure 26: Liprin-α3 as a part of the assembly mediating action potential triggered dopamine release.**

Liprin-α3 is expressed at DA release sites. Together with previosly determined assembly consisting of active zone proteins bassoon, ELKS and RIM, is mediating action potential triggered DA release. Distribution of these specialized release sites is sparse, accounting only for a limited number of DA varicosities that respond to action potential. Presence of proteins ELKS1, synaptotagmin and piccolo requires better control experiments to establish their presence at DA release sites. Source modified after: (Liu et al., 2018).

Preliminary data suggest the presence of active zone proteins ELKS1 and piccolo, however, to better establish these findings, control experiments in the form of KO/KD or transgenic animal models have to be employed. For assessment of the level of expression of isoform Liprin-α2, optimizations have to proceed further testing. Overall, the experimental approach relies to great extent on quality of antibody and its binding properties, producing and purifying better antibodies or nanobodies is challenging process covering long time span but might provide new answers.

## 4.2 Clusters of active zone proteins in cholinergic neurons

Body of evidence established that DA can be released by inputs from ChI that can trigger DA release independent of cell body firing (Cachope & Cheer, 2014; Threlfell et al., 2012). However, whether ACh is released through specialized release sites or signals in a more diffusible mode as a volume transmitter stayed an open question. Here, we suggest the insight into molecular architecture mediating ACh release for the first time. We employed confocal microscopy on striatal synaptosomes immunolabelled with antibodies recognizing vesicular transporters and antibodies recognizing active zone proteins to provide possible answers for this question. We have detected clusters of less than <20% of overlapped area between active zone proteins ELKS1/2 α, molecular scaffold bassoon and vesicular marker vAChT.

### 4.2.1 Presence of synaptic vesicles in synaptosomes labelling cholinergic neurons

In addition to active zones, our experiments tested and confirm the presence of synaptic vesicles in ChI as determined by the quantification of overlapped areas between synaptic vesicle marker synaptophysin and vesicular markers identifying the respective subtypes of neurons. Moreover, the characteristic of specialized release site on the presynaptic membrane is its opposing localization to postsynaptic membrane. The presence of postsynaptic membrane was assessed in parallel with testing for active zone proteins. Detected level of postsynaptic density followed the level of active zone proteins accounting for approximately 4-fold difference in expression in case of GABAergic neurons. In case of glutamatergic synapses, this fold

difference doubled with a possible explanation in development of excitatory and inhibitory neurons. Several electron microscopy reconstructions reported variability in inhibitory to excitatory postsynaptic density association. As well as the postsynaptic density of excitatory glutamatergic neurons is more complex and dynamic than of inhibitory GABAergic neurons (Sheng & Kim, 2011).

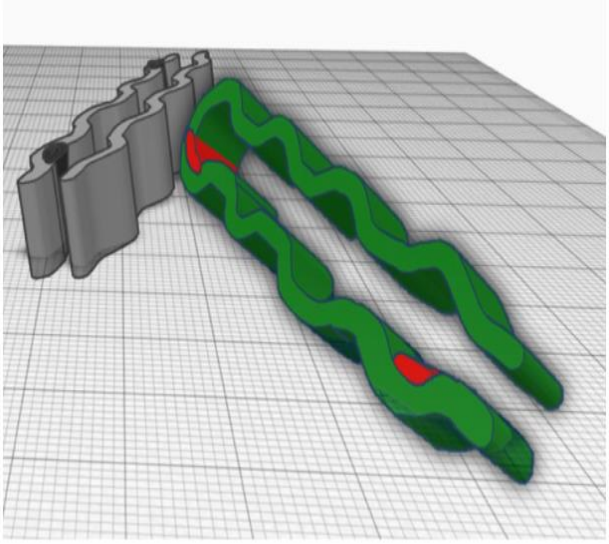

**Figure 27: Release of acetylcholine is mediated by clusters of active zone proteins bassoon and ELKS expressed at low level.**

Components of specialized release sites, active zone proteins bassoon and ELKS comprise significantly lower expression level in ChI (green) than expression level at subtypes of neurons releasing classical neurotransmitters. Illustration depicts possible distribution of active zone release sites (red) as found in dopaminergic neurons (grey) – the hypothesis set out to be tested in follow up experiments. Source: author's chart.

## 4.3 Comparison across different neuron subtypes

We have established that the release of DA regulator, neurotransmitter ACh that is binding to nicotinic receptors on DA axons, is mediated by clusters of low level of active zone proteins in cholinergic varicosities. While the absolute percentage might underestimate the actual biological representation, the relative comparison to the percentual level of active zone proteins in neurons releasing classical neurotransmitters GABA and glutamate indicates 3-4-fold difference. Unlike the release of classical neurotransmitters that requires the presence of specialized release sites for the fast release with high release probability, the release of ACh is mediated through clusters of low-level active zone proteins. The level of expression can be indirectly compared to the level detected in dopaminergic neurons. However, this provides only approximate comparison, as the marker for subset of DA neurons is DA synthetizing enzyme, whereas ChI are identified by the presence of the respective vesicular transporter. These datasets are supported by antibody verifying properties

in brain slices from transgenic animal models expressing fluorescent protein and RNA expression datasets from *in situ* hybridization and RNA single cell sequencing screened by Allen Institute for Brain Science and DropViz. Low level of specialized release hotspots in this subset of neurons might predict its more diffusible character with only small component of cholinergic varicosities responding to action potential.

## 4.4 Relevance of obtained data

Loss of dopaminergic neurons with subsequently reduced DA levels is an accompanying characteristic of Parkinson's disease (Surmeier et al., 2014). With the aging population, incidence of degenerative disorders is steadily increasing (Maiti, Manna, & Dunbar, 2017). Understanding the molecular ultrastructure of neurons is the pressing factor for therapeutic advancement and elucidation of molecular mechanisms underlying neurodegeneration. Together with translational profiling of degenerative neurons (Brichta et al., 2015), investigation of processes and structure within the basic neuroscience is providing the ground for more targeted treatment.

## 4.5 Data validity and analytical limitations

Analytical approach described in this paper provides reliable confirmation of the presence of the investigated proteins. However, it is not possible to distinguish whether the protein is not present, or the level of background staining is too high. The detected levels in KO mice represent the level of background staining or the proximity of active zones of other subsets of neurons that the resolution of confocal microscope does not allow to distinguish. It is not possible to establish negative statements about protein composition in nerve terminals based on employed analytical method.

## 4.6 Future outlook

These experiments raise further questions. Obtained data establish the presence of Liprin-α3 at DA release sites, it will be important to determine the precise nanoscale localization within a synaptic terminal using superresolution microscopy. To obtain

a full insight, Liprin-α3 will be tested for function properties in electrophysiology recordings. Furthermore, as datasets from this study suggest the presence of clusters of active zone proteins to be expressed at low level in cholinergic neurons. These specialized release sites can be distributed sparsely as in dopaminergic neurons or grouped on cholinergic axons within a distinct area. Employment of 3D SIM microscopy will reveal precise nanoscale distribution of these release sites. Generation of RIM-deficient mutant mice specifically in ChI will provide supporting answers for both obtained datasets, and open questions.

## 4.7 Concluding remarks

Neuromodulation by DA is involved in emotion, cognition and behaviour. Dysfunction of DA coding is a hallmark underlying multitude of disorders including schizophrenia and depression. Understanding the way DA is released and regulated is necessary for development of new treatment therapies. Here, we identified other protein components of molecular machinery that mediate DA release. Regulation of DA release is undertaken via firing from DA cell bodies residing in midbrain, as well as by cholinergic and glutamatergic inputs directly in the striatum. Released ACh and glutamate are binding on receptors located on DA axons. We pursued the first steps for the understanding of release of DA regulator, neurotransmitter ACh. In summary, our experiments suggest that limited number of dopaminergic varicosities is identified with the presence of active zone proteins bassoon, ELKS, RIM and Liprin-α3 that may rapidly code for information. Molecular architecture of neurons releasing DA regulator - neurotransmitter ACh - predicts its signalling to be more diffusible. Only small percentage of varicosities is identified with active zone proteins bassoon, ELKS and is opposed by postsynaptic densities.

# 5 Bibliography

Acuna, C., Liu, X., Gonzalez, A., & Sudhof, T. C. (2015). RIM-BPs Mediate Tight Coupling of Action Potentials to Ca(2+)-Triggered Neurotransmitter Release. *Neuron, 87*(6), 1234-1247. doi:10.1016/j.neuron.2015.08.027

Agnati, L. F., Zoli, M., Stromberg, I., & Fuxe, K. (1995). Intercellular communication in the brain: wiring versus volume transmission. *Neuroscience, 69*(3), 711-726.

Altrock, W. D., tom Dieck, S., Sokolov, M., Meyer, A. C., Sigler, A., Brakebusch, C., . . . Gundelfinger, E. D. (2003). Functional inactivation of a fraction of excitatory synapses in mice deficient for the active zone protein bassoon. *Neuron, 37*(5), 787-800.

Backman, C. M., Malik, N., Zhang, Y., Shan, L., Grinberg, A., Hoffer, B. J., . . . Tomac, A. C. (2006). Characterization of a mouse strain expressing Cre recombinase from the 3' untranslated region of the dopamine transporter locus. *Genesis, 44*(8), 383-390. doi:10.1002/dvg.20228

Biesemann, C., Gronborg, M., Luquet, E., Wichert, S. P., Bernard, V., Bungers, S. R., . . . Herzog, E. (2014). Proteomic screening of glutamatergic mouse brain synaptosomes isolated by fluorescence activated sorting. *EMBO J, 33*(2), 157-170. doi:10.1002/embj.201386120

Boyken, J., Gronborg, M., Riedel, D., Urlaub, H., Jahn, R., & Chua, J. J. (2013). Molecular profiling of synaptic vesicle docking sites reveals novel proteins but few differences between glutamatergic and GABAergic synapses. *Neuron, 78*(2), 285-297. doi:10.1016/j.neuron.2013.02.027

Brichta, L., Shin, W., Jackson-Lewis, V., Blesa, J., Yap, E. L., Walker, Z., . . . Greengard, P. (2015). Identification of neurodegenerative factors using translatome-regulatory network analysis. *Nat Neurosci, 18*(9), 1325-1333. doi:10.1038/nn.4070

Cachope, R., & Cheer, J. F. (2014). Local control of striatal dopamine release. *Front Behav Neurosci, 8*, 188. doi:10.3389/fnbeh.2014.00188

Cachope, R., Mateo, Y., Mathur, B. N., Irving, J., Wang, H. L., Morales, M., . . . Cheer, J. F. (2012). Selective activation of cholinergic interneurons enhances

accumbal phasic dopamine release: setting the tone for reward processing. *Cell Rep, 2*(1), 33-41. doi:10.1016/j.celrep.2012.05.011

Dani, A., Huang, B., Bergan, J., Dulac, C., & Zhuang, X. (2010). Superresolution imaging of chemical synapses in the brain. *Neuron, 68*(5), 843-856. doi:10.1016/j.neuron.2010.11.021

Grace, A. A. (2016). Dysregulation of the dopamine system in the pathophysiology of schizophrenia and depression. *Nat Rev Neurosci, 17*(8), 524-532. doi:10.1038/nrn.2016.57

Hirase, H., Iwai, Y., Takata, N., Shinohara, Y., & Mishima, T. (2014). Volume transmission signalling via astrocytes. *Philos Trans R Soc Lond B Biol Sci, 369*(1654), 20130604. doi:10.1098/rstb.2013.0604

Jones, I. W., Bolam, J. P., & Wonnacott, S. (2001). Presynaptic localisation of the nicotinic acetylcholine receptor beta2 subunit immunoreactivity in rat nigrostriatal dopaminergic neurones. *J Comp Neurol, 439*(2), 235-247.

Kabat, E. A. (1980). Basic principles of Antigen-Antibody Reactions. *Methods Enzymol, 70*(A), 3-49.

Kobayashi, T., Kato-Itoh, M., Yamaguchi, T., Tamura, C., Sanbo, M., Hirabayashi, M., & Nakauchi, H. (2012). Identification of rat Rosa26 locus enables generation of knock-in rat lines ubiquitously expressing tdTomato. *Stem Cells Dev, 21*(16), 2981-2986. doi:10.1089/scd.2012.0065

Liu, C., Kershberg, L., Wang, J., Schneeberger, S., & Kaeser, P. S. (2018). Dopamine Secretion Is Mediated by Sparse Active Zone-like Release Sites. *Cell, 172*(4), 706-718 e715. doi:10.1016/j.cell.2018.01.008

Maiti, P., Manna, J., & Dunbar, G. L. (2017). Current understanding of the molecular mechanisms in Parkinson's disease: Targets for potential treatments. *Transl Neurodegener, 6*, 28. doi:10.1186/s40035-017-0099-z

Mutch, S. A., Kensel-Hammes, P., Gadd, J. C., Fujimoto, B. S., Allen, R. W., Schiro, P. G., . . . Chiu, D. T. (2011). Protein quantification at the single vesicle level reveals that a subset of synaptic vesicle proteins are trafficked with high precision. *J Neurosci, 31*(4), 1461-1470. doi:10.1523/JNEUROSCI.3805-10.2011

Nagy, A. (2000). Cre recombinase: the universal reagent for genome tailoring. *Genesis, 26*(2), 99-109.

Paddock, S. W. (1999). Confocal laser scanning microscopy. *Biotechniques, 27*(5), 992-996, 998-1002, 1004. doi:10.2144/99275ov01

Paddock, S. W. (2000). Principles and practices of laser scanning confocal microscopy. *Mol Biotechnol, 16*(2), 127-149. doi:10.1385/MB:16:2:127

Paddock, S. W., & Eliceiri, K. W. (2014). Laser scanning confocal microscopy: history, applications, and related optical sectioning techniques. *Methods Mol Biol, 1075*, 9-47. doi:10.1007/978-1-60761-847-8_2

Paes, G., Habrant, A., & Terryn, C. (2018). Fluorescent Nano-Probes to Image Plant Cell Walls by Super-Resolution STED Microscopy. *Plants (Basel), 7*(1). doi:10.3390/plants7010011

Pardon, E., Laeremans, T., Triest, S., Rasmussen, S. G., Wohlkonig, A., Ruf, A., . . . Steyaert, J. (2014). A general protocol for the generation of Nanobodies for structural biology. *Nat Protoc, 9*(3), 674-693. doi:10.1038/nprot.2014.039

Saunders, A., Macosko, E., Wysoker, A., Goldman, M., Krienen, F., de Rivera, H., . . . McCarroll, S. A. (2018). A Single-Cell Atlas of Cell Types, States, and Other Transcriptional Patterns from Nine Regions of the Adult Mouse Brain. *bioRxiv*, 299081. doi:10.1101/299081

Schenck, S., Kunz, L., Sahlender, D., Pardon, E., Geertsma, E. R., Savtchouk, I., . . . Dutzler, R. (2017). Generation and Characterization of Anti-VGLUT Nanobodies Acting as Inhibitors of Transport. *Biochemistry, 56*(30), 3962-3971. doi:10.1021/acs.biochem.7b00436

Serra-Pages, C., Medley, Q. G., Tang, M., Hart, A., & Streuli, M. (1998). Liprins, a family of LAR transmembrane protein-tyrosine phosphatase-interacting proteins. *J Biol Chem, 273*(25), 15611-15620.

Sheng, M., & Kim, E. (2011). The postsynaptic organization of synapses. *Cold Spring Harb Perspect Biol, 3*(12). doi:10.1101/cshperspect.a005678

Spangler, S. A., Jaarsma, D., De Graaff, E., Wulf, P. S., Akhmanova, A., & Hoogenraad, C. C. (2011). Differential expression of liprin-alpha family proteins in the brain suggests functional diversification. *J Comp Neurol, 519*(15), 3040-3060. doi:10.1002/cne.22665

Spangler, S. A., Schmitz, S. K., Kevenaar, J. T., de Graaff, E., de Wit, H., Demmers, J., . . . Hoogenraad, C. C. (2013). Liprin-alpha2 promotes the presynaptic recruitment and turnover of RIM1/CASK to facilitate synaptic transmission. *J Cell Biol, 201*(6), 915-928. doi:10.1083/jcb.201301011

Sudhof, T. C. (2012). The presynaptic active zone. *Neuron, 75*(1), 11-25. doi:10.1016/j.neuron.2012.06.012

Sunkin, S. M., Ng, L., Lau, C., Dolbeare, T., Gilbert, T. L., Thompson, C. L., . . . Dang, C. (2013). Allen Brain Atlas: an integrated spatio-temporal portal for exploring the central nervous system. *Nucleic Acids Res, 41*(Database issue), D996-D1008. doi:10.1093/nar/gks1042

Surmeier, D. J., Graves, S. M., & Shen, W. (2014). Dopaminergic modulation of striatal networks in health and Parkinson's disease. *Curr Opin Neurobiol, 29*, 109-117. doi:10.1016/j.conb.2014.07.008

Tabll, A., Abbas, A. T., El-Kafrawy, S., & Wahid, A. (2015). Monoclonal antibodies: Principles and applications of immmunodiagnosis and immunotherapy for hepatitis C virus. *World J Hepatol, 7*(22), 2369-2383. doi:10.4254/wjh.v7.i22.2369

Threlfell, S., Lalic, T., Platt, N. J., Jennings, K. A., Deisseroth, K., & Cragg, S. J. (2012). Striatal dopamine release is triggered by synchronized activity in cholinergic interneurons. *Neuron, 75*(1), 58-64. doi:10.1016/j.neuron.2012.04.038

Tritsch, N. X., Ding, J. B., & Sabatini, B. L. (2012). Dopaminergic neurons inhibit striatal output through non-canonical release of GABA. *Nature, 490*(7419), 262-266. doi:10.1038/nature11466

Wang, S. S. H., Held, R. G., Wong, M. Y., Liu, C., Karakhanyan, A., & Kaeser, P. S. (2016). Fusion Competent Synaptic Vesicles Persist upon Active Zone Disruption and Loss of Vesicle Docking. *Neuron, 91*(4), 777-791. doi:10.1016/j.neuron.2016.07.005

Whittaker, V. P., Michaelson, I. A., & Kirkland, R. J. (1964). The separation of synaptic vesicles from nerve-ending particles ('synaptosomes'). *Biochem J, 90*(2), 293-303.

Wilhelm, B. G., Mandad, S., Truckenbrodt, S., Krohnert, K., Schafer, C., Rammner, B., . . . Rizzoli, S. O. (2014). Composition of isolated synaptic boutons reveals the amounts of vesicle trafficking proteins. *Science, 344*(6187), 1023-1028. doi:10.1126/science.1252884

Wong, M. Y., Liu, C., Wang, S. S. H., Roquas, A. C. F., Fowler, S. C., & Kaeser, P. S. (2018). Liprin-alpha3 controls vesicle docking and exocytosis at the active zone of hippocampal synapses. *Proc Natl Acad Sci U S A, 115*(9), 2234-2239. doi:10.1073/pnas.1719012115

Zhong, G., Reis e Sousa, C., & Germain, R. N. (1997). Production, specificity, and functionality of monoclonal antibodies to specific peptide-major histocompatibility complex class II complexes formed by processing of exogenous protein. *Proc Natl Acad Sci U S A, 94*(25), 13856-13861.

Zurner, M., Mittelstaedt, T., tom Dieck, S., Becker, A., & Schoch, S. (2011). Analyses of the spatiotemporal expression and subcellular localization of liprin-alpha proteins. *J Comp Neurol, 519*(15), 3019-3039. doi:10.1002/cne.22664

# 6 Annex

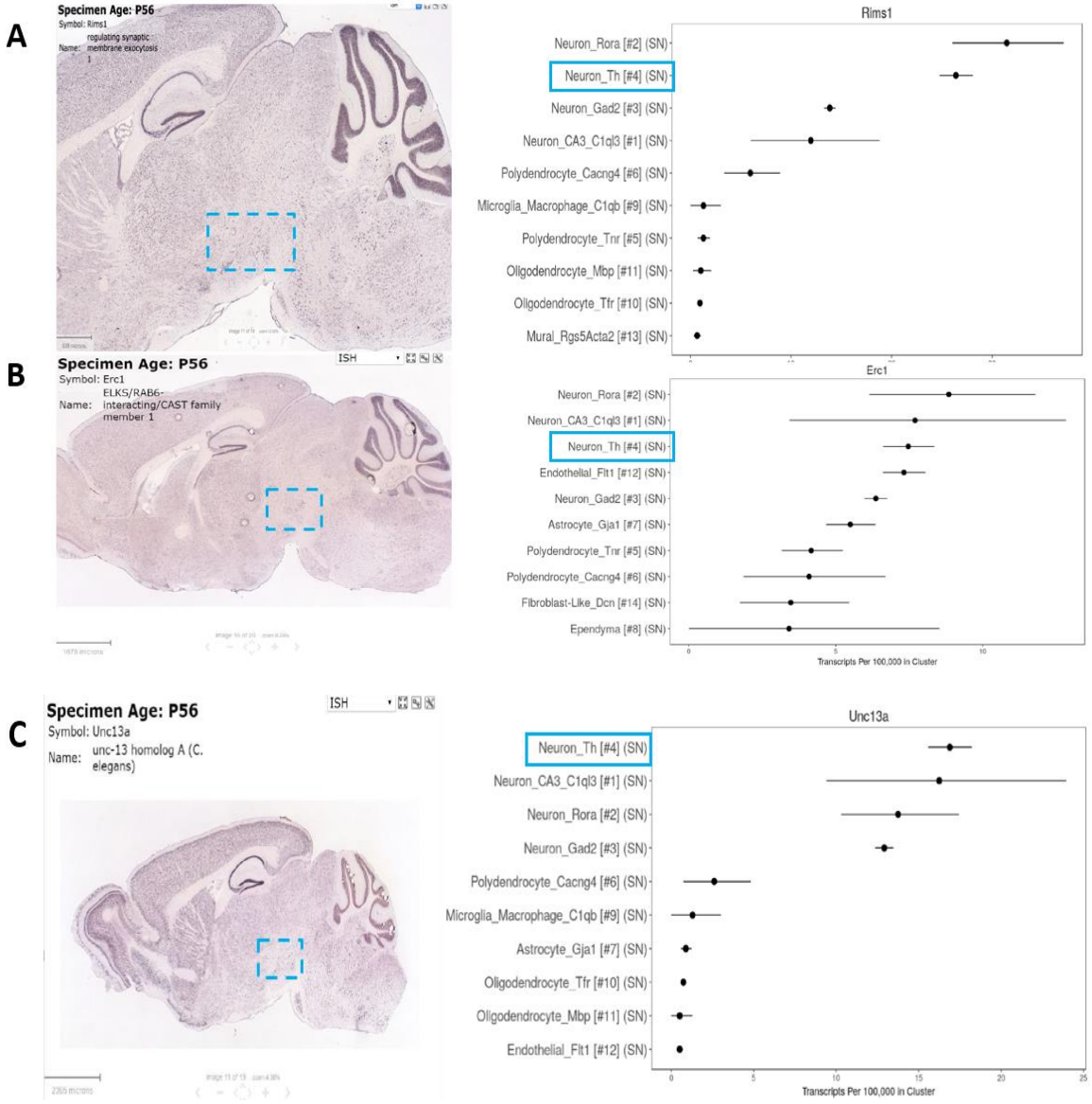


**Figure 28: RNA transcriptome viewed in saggital slices and RNA micorarray**

High resolution images of saggital brain slices after *in situ* hybridization and RNA micorarray data for active zone proteins RIM (A), ELKS1 (B), Munc13 (C). Approximate area of the investigated brain region indicated in blue. Source modified after: “Allen Brain Atlas”, http://www.brain-map.org and “DropViz”, http://dropviz.org/.

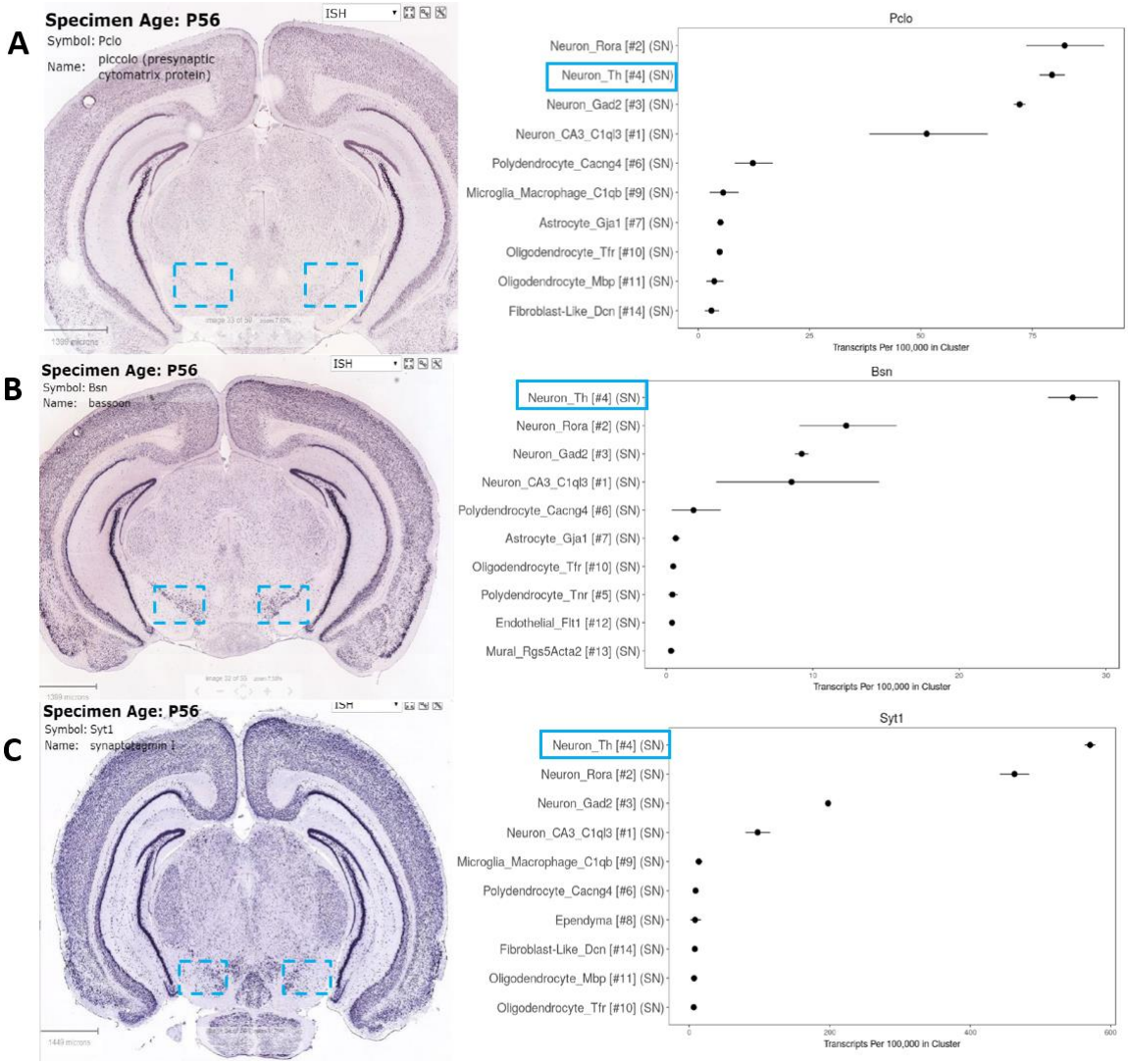


**Figure 29: RNA transcriptome viewed in coronal slices and RNA micorarray**

High resolution images of coronal brain slices after *in situ* hybridization and RNA micorarray data for active zone proteins piccolo (A), bassoon (B), and calcium sensor synaptotagmin1 (C). Approximate area of the investigated brain region indicated in blue. Source modified after: “Allen Brain Atlas”, http://www.brain-map.org and “DropViz”, http://dropviz.org/.